Renewable Energy 125 (2018) 1–20

Contents lists available at ScienceDirect

Renewable Energy

journal homepage: www.elsevier.com/locate/renene

Air-cooled fuel cells: Keys to design and build the oxidant/cooling system

A. De las Heras*, F.J. Vivas, F. Segura, M.J. Redondo, J.M. Andújar

Grupo de Investigación de Control y Robótica TEP-192, Departamento de Ingeniería Electrónica, de Sistemas Informáticos y Automática, Escuela Técnica Superior de Ingeniería, Universidad de Huelva.Carretera Huelva, Palos de la Frontera, 21819, La Rábida, Palos de la Frontera, Huelva, Spain

ARTICLE INFO

Article history:
Available online 19 February 2018

Keywords:
Air cooled polymer electrolyte fuel cell
BoP configurations
Oxidant/cooling subsystem design
Experimental study
Performance improvement

ABSTRACT

In the field of energy, hydrogen as an energetic vector is becoming increasingly important. Specifically, fuel cells powered by hydrogen are becoming an alternative in automotive and other fields because of their ability to produce electricity without any pollution. Therefore, at this time there is a very active research field. A fuel cell can be described as a scale down industrial plant that consists of different subsystems whose purpose is to make the stack works properly. Air Cooled Polymer Electrolyte Fuel Cells (AC-PEFC) are receiving special attention due to their potential to integrate the oxidant and cooling subsystems into one, which in term gives the fuel cells their capability to reduce its weight, volume, cost and control complexity. In these fuel cells, the Oxidant/Cooling subsystem is of crucial importance and along with three others (*Fuel*, *Electrical* and *Control* subsystems) make up the Balance of Plant (BoP), which together with the stack comprise the full fuel cell system. The aim of this paper is to present a comprehensive experimental study of an AC-PEFC paying particular attention to the Oxidant/Cooling subsystem configuration. According to the scientific literature, this subsystem has not received the same attention as other subsystems like the *Fuel* and *Control* subsystems. However, a suitable design and size is critical for the proper functioning of the stack. The analysis carried out in this paper tries to solve some problems that can appear if the design of the Oxidant/Cooling subsystem has not been optimized. These problems are related to important aspects such as the performance and the efficiency of the whole system and temperature distribution over the stack.

1. Introduction

Polymer Electrolyte Fuel Cells (PEFCs) are a promising technology to produce electricity from hydrogen for stationary power generation due to its operational strength such as high power density, low operating temperature, low corrosion, quiet operation, stack design simplification, relatively quick start up and shut down and especially by its zero emission capability [1–4]. In the past decades, there has been a huge progress in the PEFC field but researchers are still focused on new cell designs, cost reduction and performance improvement. PEFC technology is having more and more importance because it is suitable for a wide range of applications, including portable, stationary and automotive power delivery [5–8] and lately it is being more used in backup systems for emergency situations (e.g. earthquakes, terrorist attacks). Configuration or hybridization of generation systems around the PEFC can be miscellaneous [6] [7,9], as well as its control modes [10].

For the configuration of a PEFC system, apart from the stack it is necessary to include additional subsystems for the proper system operation. Generally these systems can be divided into five main groups which form the Balance of Plant (BoP): 1- Oxidant subsystem: it supplies air/oxygen at the appropriate conditions for the oxidant reaction, 2-Fuel subsystem: it supplies hydrogen at the appropriate conditions for the reduction reaction, 3-Cooling subsystem: it removes the heat produced in the stack and keeps it at the temperature recommended by the manufacturer and removes the water produced, 4-Electrical subsystem: it connects the stack to electric load, and 5-Control subsystem: it processes information from sensors so as to control the actuators, Fig. 1 [11–13].

When it comes to develop a PEFC system, researchers conclude that an appropriate design of the BoP is essential to the proper PEFC stack operation and influences on the performance of the whole system. Therefore, according to the BoP design, it is important to

* Corresponding author.
E-mail address: ainhoa.delasherasjimenez@gmail.com (A. De las Heras).

https://doi.org/10.1016/j.renene.2018.02.077
0960-1481/

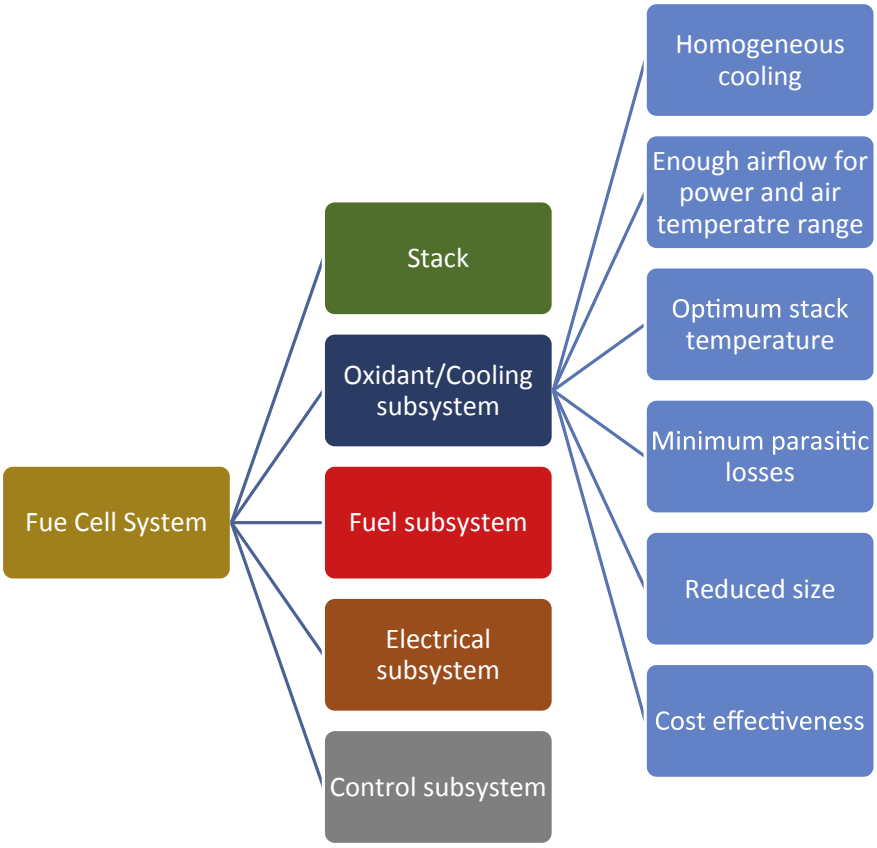

Fig. 1. Conceptual scheme of an AC-PEFC system and challenges in the design and manufacture of the oxidant/cooling subsystem.

optimize the main subsystems avoiding an oversized BoP configuration which usually results in an increase of parasitic losses, system volume, weight and noise level [14].

While the PEFC is operating, the stack temperature changes along the time and with the load demand. The temperature has influence on electrochemical reaction rate and water and reactant transport. Low temperatures might produce membrane flooding and because of that, it might appear operating problems due to membrane resistivity variation. Otherwise, high temperatures might produce membrane thermal stress and cathode catalyst inactivity, resulting in membrane degradation. In basis on this, we can deduce that the Cooling subsystem plays an important role for reliable and efficient stack operation, besides the few papers found in the scientific literature focused in this question [13].

In this work, authors we develop the experimental study using an Air Cooled Polymer Electrolyte (AC-PE) stack. This kind of stacks integrates Oxidant and Cooling subsystems into one single avoiding the liquid parts in the Cooling subsystem. This results in facilitating and simplifying the BoP integration because they do not need pipes, valves, pumps and heat exchangers, contributing to reduce weight, volume and cost. Apart from this, the stack used in this work does not require high inlet hydrogen pressure (it can operate near ambient pressure) and this provides security because it is not necessary to operate with high hydrogen supply pressures and less stringent requirements in the hydrogen transfer circuit (connections, pipelines, etc.).

The implementation of the Oxidant/Cooling subsystem is commonly based on a forced-air convection design with one or several fans. This design requires especial consideration of the stack characteristic curves and the fan/s. Ideally, the operating point intersection between the stack and the fan characteristic curves should be located in the optimal operating region of the fan; and be sufficiently far away from any unstable region [15].

Different BoP configurations have been developed in several works [13,16–25], and the chosen configuration is justified in basis on the required particular conditions by the authors. However, there are not too many works in which different configurations are analysed, discussing their advantages and disadvantages. Thus, Kim et al. [26] show two types of Oxidant/Cooling subsystems (a gas recirculation subsystem with and without a recycle blower). Sasmito et al. [15] present a model in which the results indicate that some factors such as fan power and type, single fan or fans in series, stack length, and separate air-coolant channels have a significant impact on the operating point and the stack performance. Meyer et al. [27] point out that in an cathode AC-PEFC, the air blowers present the largest parasitic load having a direct influence on the stack performance and its temperature.

Based on the bibliography consulted to establish the state of the art of this paper and in our own experience of more than 10 years dealing with PEFCs, we can set six challenges in the design and manufacture of the oxidant/cooling subsystem (Fig. 1): 1) To be able to cool the stack homogeneously, 2) To provide sufficient airflow range to control the PEFC temperature, under a range of power and room/coolant air temperature, 3) To place the stack at optimum temperature, 4) To reduce the auxiliary power consumption, 5) To do all this within a certain sized box, and finally but not least important 6) To do it cost effectively.

In this paper, authors try to expand the current experimental studies published in the scientific literature, and they present a detailed experimental analysis of three different configurations for the Oxidant/Cooling subsystem in an AC-PEFC.

Our study departs from one configuration based on the own

stack's manufacturer proposal. From here, we raise two new configurations to enhance the initial, including different ways of controlling the fan/s contained within the configurations. As it has been reported in previous works [27], the operating performance of this class of PEFCs is conditioned by the coolant air-flow rate, because both the air flow and the room air temperature determine the operating temperature of a given air-cooled fuel cell, at a certain power output. Then the study developed in this paper allow us to analysis what configuration guarantees a better system performance, attending to those six challenges presented in Fig. 1, at time that the stack achieves the highest power working inside its operating temperature range and air stoichiometric rate. Moreover, this experimental study will show us what configuration requires a lowest number of devices or the most complex control system. Additionally, once the best configuration has been identified, it has been checked at different room temperatures to prove it guarantees the oxidant/cooling requirements by the stack.

The structure of the paper is as follow: Section 2 exposes the main features of the test bench developed by authors and used during all the experimental tests. Section 3 presents the proposed Oxidant/Cooling subsystem designs, pointing out the particularities of each one. Next, experimental results obtained from each configuration as well as some discussions about them are summarised in Section IV and V respectively. Finally, Section 6 draws the main conclusions derived from the experimental study.

2. Materials and methods

The test bench for this study (an AC-PEFC system) has been design and built around an air-cooled FCgen-1200ACS stack model from Ballard®, Fig. 2. Additionally, Table 1 summarizes the stack experimental parameters.

The used stack does not need external air humidification and it has a dead-end operation mode; it is used with dry hydrogen without humidification as well. The inlet hydrogen pressure can be varied from 1.16 to 1.56 bars. The stack is made up by 80 cells and it can reach up to 3.4 kW, according to manufacturer's data [28,29]. This stack has been integrated with a BoP configuration developed by authors according to [16]; the instrumentation specifications can be accessed in Table 2. The system shown in Fig. 2 presents a handy test bench to carry out all kinds of tests on a medium power

Table 1
Stack experimental parameters.

Variable	Definition	Range
V_{cell} (V)	Cell Voltage	0.647–1.005
I_S (A)	Stack Current	0–75
T_{opt} (°C)	Optimal Operating Temperature	26.01–65.76
T_S (°C)	Stack Temperature	6–75
T_{in} (°C)	Inlet Air Temperature	10–40
Q_{stack} (slpm)	Stack Required Air flow	0–18656.63
Q_{cell} (slpm)	Cell Required Air Flow	0–237.20
q_{cell} (W)	Heat Produced by Cell	0–45.56
E (V)	Max. Cell Voltage product water vapor	1.2545
λ	Inlet Air Flow/Consumed Air Flow	20–200
C (slpm) slpm/A*cell	Air Cell Consumption	0.0167
n_{cell}	Number of cells	80
RH/%	Relative Humidity	5–100
P_{H2} (kPa)	Inlet Hydrogen Pressure	116–156

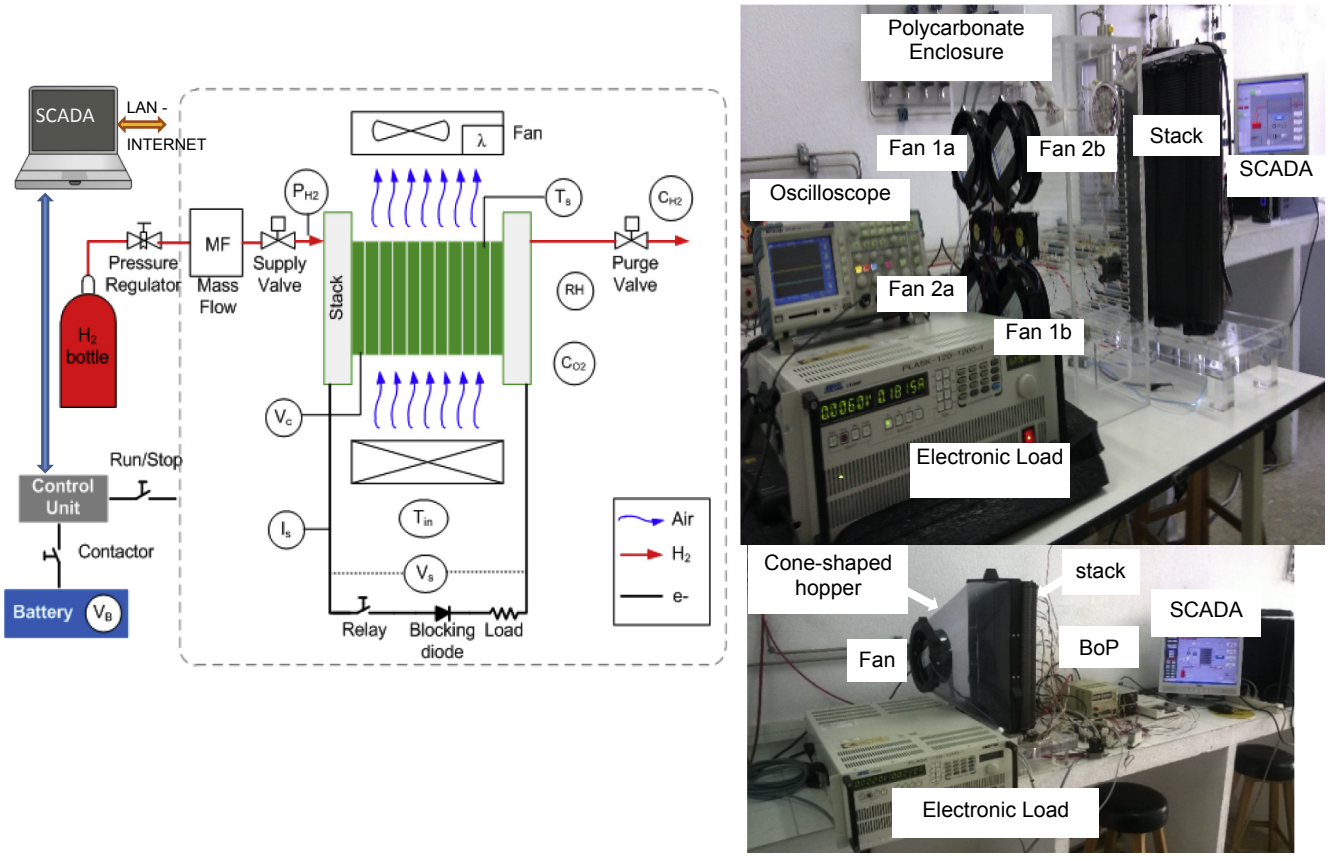

a) Test bench diagram. b) Up and c) Down. Oxidant/Cooling subsystem configurations.

Fig. 2. Diagram and real implementation of the test bench for AC-PEFCs.

Table 2
Instrumentation specifications.

Component	Manufacturer-Model	Quantity
Fuel cell stack	Ballard-FCS1020ACS	1
Oxidant/Cooling Subsystem		
Fan	Embpast-6224TD (Configuration 1 and 2)	4
	Embpast-6224TDA (Configuration 3)	1
Inlet air temperature sensor	Burkert-8400 Accuracy ± 1.5%	1
Fuel cell temperature sensor	Maruta P/N NCP15WF104F03RC Accuracy ± 1%	Included in stack
Oxigen sensor	Figaro-KE50, Accuracy ± 1%	1
Fuel Subsystem		
Valve supply	Burkert-6013	1
Purge valve	Burkert-6606	1
Pressure sensor	Burkert-8314, Accuracy ± 0.3%	1
Hydrogen sensor	Figaro-FCM6812, Accuracy ± 0.2%	1
Electrical Subsystem		
Current sensor	LEM LA 55-P, Accuracy ± 0.9%	1
Stack voltage sensor	LEM-LV 25-P, Accuracy ± 0.8%	
Bloking diode	Vishay-T85HFL	1
Relay	Panasonic-AEV18012	1
Control system		
Microprocessor	Arduino ATMega256	1
Battery	Exide-GF 12 094 Y	1

real AC-PEFCs [16].

Paying special attention to the Oxidant/Cooling subsystem (blue line in Fig. 2a), it includes an adjustable flow fan, an inlet air temperature sensor (T_{in}), and a stack temperature sensor (Ts) built-in the own stack. The manufacturer only includes a stack temperature sensor in the own stack and thermographies of the stack are not facilitated in the manuals. The air stoichiometric coefficient (λ) must be adjusted by the control unit to optimize the system performance. Additionally, a concentration oxygen sensor (C_{O2}) is included to prevent low concentrations of oxygen in the surrounding atmosphere, and a relative humidity sensor (RH) to avoid operating under overly dry room conditions.

Following Fig. 2a, at the fuel input, the Fuel subsystem (red line) is composed by the hydrogen storage bottle, and a manual pressure regulator to reduce the high pressure from the bottle up to the pressure range recommended by the manufacturer's data. In addition it is available a mass flow meter to measure the hydrogen consumption, a supply valve to control the hydrogen entry and a hydrogen pressure sensor (P_{H2}) to measure the inlet anode pressure forming the hydrogen input line. In the hydrogen outlet, although the used stack for tests is designed for dead-ended operation, that is all the fuel enters the anode is used up (fuel stoichiometry: 1), in practice water vapor, nitrogen and other inert gases can be collected in the anode, so this side must be purged periodically. For this reason, a purge valve avoids the accumulation of inert gases for a proper operation of the system and to prevent unsafe room conditions. Finally, a concentration hydrogen sensor (C_{H2}) has been included.

The Electrical subsystem (black line in Fig. 2a) comprises a stack current sensor (Is), stack voltage sensor (Vs) and a cells voltage measurement system (Vc). Additionally, a relay is added to isolate the fuel cell system from the electronic load and a blocking diode to avoid reversal currents.

In addition to the above elements and in order to make all test bench subsystems works properly, with the aim to get the best performance of the stack, a control unit has been developed. It takes care of receiving all the information from sensors and decides what to do every moment: to open the supply valve, to open the purge valve, to run the fan, to connect or disconnect the electrical load, and so on.

On the other hand, it is necessary to note that the system does not produce electricity instantaneously, even more during the start-up the stack can't provide electrical power but the BoP needs to be supply. Therefore, an auxiliary source needed to guarantee the electrical supply to BoP. This is the role of the battery shown in Fig. 2a, where the battery voltage sensor V_B warns of its state.

At this point, it is very important to mention that the management of the test bench requires a complex control system. To this end, a supervisory control and data acquisition (SCADA) has been developed. Its function is to carry out the high-level supervisory management of the test bench. It is hosted in a PC and it is provided with a data network connection for remote management, as well as graphical user interfaces. It can also manage others peripheral devices (PIDs, sensors, actuators and so on) by the control unit (see Fig. 2a). This means that, by the SCADA, we can have absolute control of the test bench as well as process all its information.

Fig. 2b and c represent the real configurations of the test bench where this experimental study will be carried out. These configurations are the result of a design analysis which will be discussed below.

Finally, to conclude this section, we must mention that the thermographies shown in this paper has been made with a TESTO® 875-1i camera, with a matrix of 120 × 160 sensors and a thermal resolution (NETD) < 50 mK. Temperature range: −30 °C to +100 °C.

3. Oxidant/cooling subsystem designs

Now, after the explanation in the previous section of the features of the test bench (AC-PEFC system), different Oxidant/Cooling subsystem architectures will be designed and built. Taking into account the manufacturer's recommendation, uniform flow rate is achieved by using fans to pull air through the stack instead of mounting fans at the air inlet and blowing air through the stack. This allows the negative pressure zone created at the air outlet will act to distribute airflow evenly through the stack, eluding the flooding phenomena [29]. With this way of working of the fans, it is assumed that the phenomenon of flooding will not appear, because the supplied air is sufficient to avoid it. The configuration of each one are the following:

- Configuration 1: Four fans covering the cathode area of the stack working two by two without flow control.
- Configuration 2: Four fans covering the cathode area of the stack working two by two with flow control.
- Configuration 3: One single speed controlled fan.

For configurations 1 and 2, with 4 fans (Fig. 2b), authors have proposed their designs in basis on stack's manufacturer recommendations [28,29]. Manufacturer advices to use one single fan for stack sizes of 45 cells or less (Fig. 3a), and two fans in other case (remember that the stack under study has 80 cells). For stack sizes higher than 45 cells the diagram for the fans stand proposed by manufacturer is shown in Fig. 3b, standard configuration, [29]. Then according to these recommended designs, authors have minimally changed it with the aim to improve the Oxidant/Cooling subsystem that is the stack air-breathing system. Putting four fans instead of two, a higher coverage of the stack cathode is guaranteed so the air can arrive at the cells located both at the top and bottom, and at the ends rightmost and leftmost of each cell. This can be seen in Fig. 2b and it has been built over a polycarbonate rectangular-shaped enclosure. The fans selection has been done in basis on the air stoichiometric requirements of the stack [15,16] and they correspond to fan model EbmPapst® DV6224TD. This enclosure has been used to stand the four fans that integrate the Oxidant/Cooling subsystem.

Regarding configuration 3 with only a fan, the aim of the authors has been to improve the air breathing of the stack and its temperature distribution over the cathode. This third configuration tries to sort out the problem observed in configurations 1 and 2: the air follow preferential paths surrounding the stack instead of crossing it for its cooling.

To carry out the configuration 3, a cone-shaped hopper has been designed and built. This additional tool allows to canalise the air flow in the best homogeneous way as possible (Fig. 2c), forcing the air to blow through the stack instead of surrounding it. Additionally, it has been put properly around the stack without leaving any space between the stack and the hopper avoiding preferential paths of the air flow.

The homogeneous flow is got minimizing the turbulence which will occur in the exit of the flow adapter. To select the high of the hopper (distance between the stack and the fan), authors have compared three possible distances: 20 cm, 25 cm and 30 cm. Experimental results obtained from the three cases are practically the same.

The fan selection has been done in basis on the air stoichiometric requirements of the stack [15,16], and it consists on the adjustable flow fan model EbmPapst® DV6224TDA. The chosen fan is capable of withstanding the maximum pressure drop and supplying the maximum air flow required by system [30].

In summary, regarding to the first two configurations, the third presents two changes to try to enhance the Oxidant/Cooling subsystem. The first change is it uses one single fan instead of four, simplifying the design, minimizing the BoP cost and weight and reducing the auxiliary power consumption and the control complexity. The second change is to use a flow adapter (cone-shaped hopper) instead of a rectangular-shaped enclosure avoiding preferential paths.

Figs. 4–6 represent in schematic form the mode of operation for each of the configurations. In Fig. 4 (configuration 1) the four fans are divided into two groups (GROUP 1-fans in blue line and GROUP 2-fans in orange line). The first group of fans is always working when the fuel cell system is operating and the second group of fans starts to work in case of the stack temperature is higher than the optimal temperature value. The optimal temperature value depends on the operating point in which the stack is operating and according to manufacturer data [28,29].

Fig. 5 represents the second configuration, which is similar to the first one (the actual assembly is again Fig. 2b) but in this case, both groups of fans will be controlled in basis on the difference between the real stack temperature value and the optimal stack temperature value recommended by the manufacturer.

Finally, Fig. 6 represents the last configuration with a flow adapter (cone-shaped hopper) and a speed adjustable fan.

4. Experimental results

The different configurations designed have been implemented on the test bench, as shown in Fig. 2. Once the test bench is set up for each configuration, its SCADA governs, by the control unit, all the Oxidant/Cooling subsystem operation (and in general all the fuel cell subsystems and their operations) in each configuration. From it, you can set setpoints; capture, process and show all data, in different ways and in different formats. In the following, we will discuss the results obtained for each Oxidant/Cooling subsystem configuration.

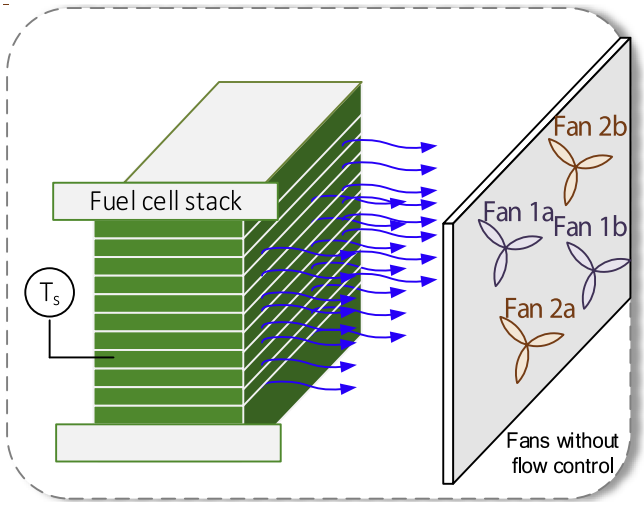

Fig. 4. Configuration 1: Four fans working two by two without flow control.

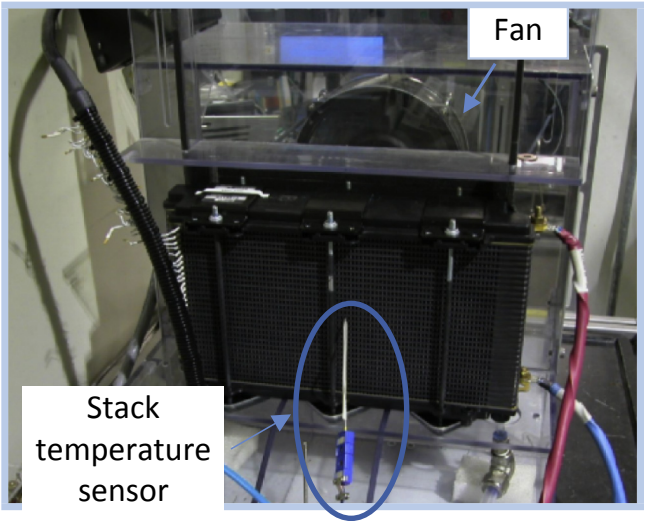

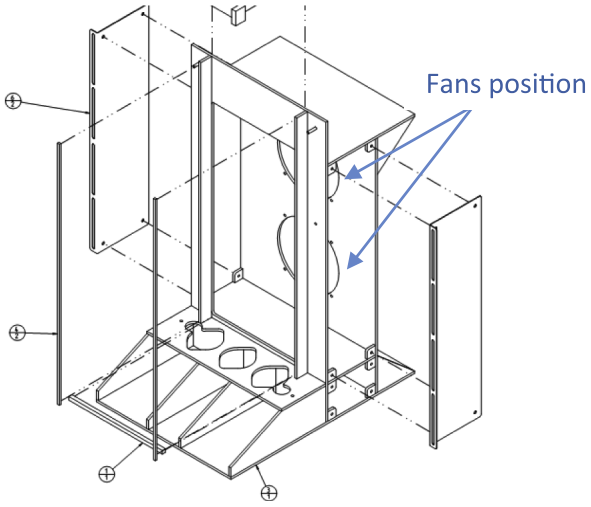

Fig. 3. a. Fan enclosure proposed by manufacturer for stack sizes equal or lower than 45 cells (standard configuration) Fig. 3b. Fan stand design proposed by manufacturer for stack sizes higher than 45 cells (standard configuration).

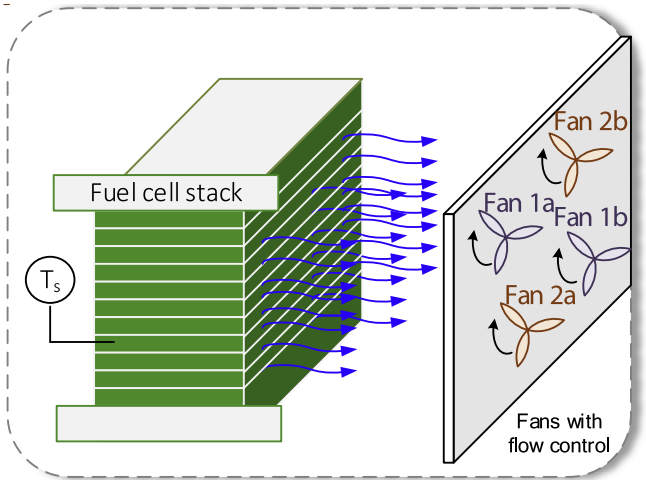

Fig. 5. Configuration 2: Four fans working two by two with flow control.

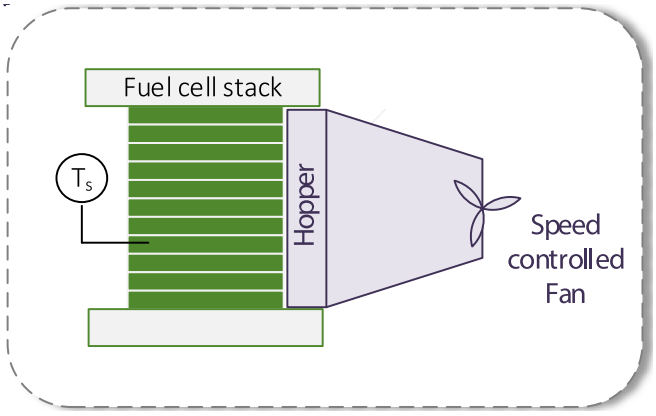

Fig. 6. Configuration 3: One single speed controlled fan inside a cone-shaped hopper.

a) Configuration 1: Four fans covering the cathode area of the stack working two by two without flow control.

For this configuration, the test bench is set up as in Fig. 2b. Fig. 8 shows the flow chart of the operation with this configuration. The experimental analysis starts comparing the real stack temperature with the optimal and robust stack temperature recommended by the manufacturer, expression (1) and (2) respectively, [29].

$$Topt = 0.46\, I_{stack} + 33.63 \quad (1)$$

$$Trob = 0.53\, I_{stack} + 26.01 \quad (2)$$

where,

Topt : Optimal stack temperature (ºC) recommended by manufacturer for legacy operating conditions (air inlet temperature from 10 °C to 40 °C).
Trob: Optimal stack temperature (ºC) recommended by manufacturer for robust operation over wide air inlet temperature range (−20 °C–52 °C). Keeping the stack near this operating temperature, the stack performance and cell stability are achieved.

The aim to compare the real stack temperature with optimal and robust temperature provided by the manufacturer, it is to show that oxidant configurations proposed in this work satisfies $Trob < T_{real} <$

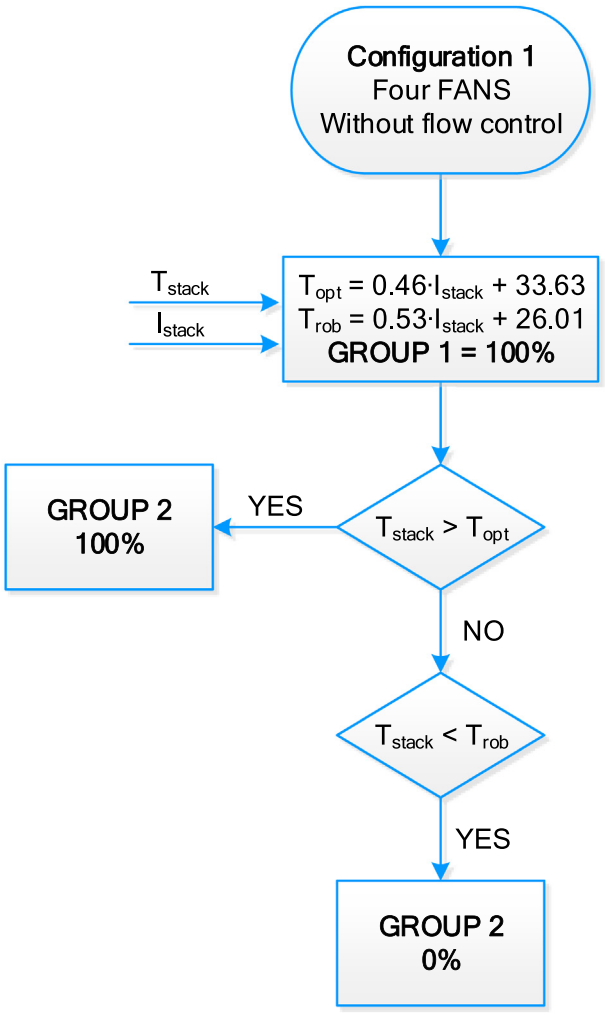

Fig. 7. Flow chart of configuration 1: Four fans working two by two without flow control.

T_{opt} even when initial room temperature is below stack temperature (it is also called *cold start*).

Then, according to the control logic shown in Fig. 7, the first group of fans is always working, and if the stack temperature is higher than the optimal stack temperature at the actual stack current value, the second groups of fans starts to work as well. However if the stack temperature is lower than optimal temperature and also lower than the robust temperature, the control unit does not put in work the second group of fans, keeping in operation only the first one. This situation corresponds with the case where the stack temperature is near the recommended values and the stack operates under acceptable operating conditions. In this case, the first group of fans is kept in operation because they are needed to supply the airflow required by the electrochemical reaction in the stack. In this configurations, fans operating mode is ON/OFF. This means that all the fans will be working at the maximum accepted value, without any control over the fan speed. As an advantage of this configuration, we can highlight its simplicity, but it cannot offer the possibility to adjust the air stoichiometry rate.

Next, we are going to analyse the fuel cell response attending to stack temperature, hydrogen pressure, voltage, current and power supplied by the fuel cell. To do this the AC-PEFC has been subjected to a multi steps load profile (10 A–30 A – 50 A).

Comparing the stack temperature with the optimal and robust

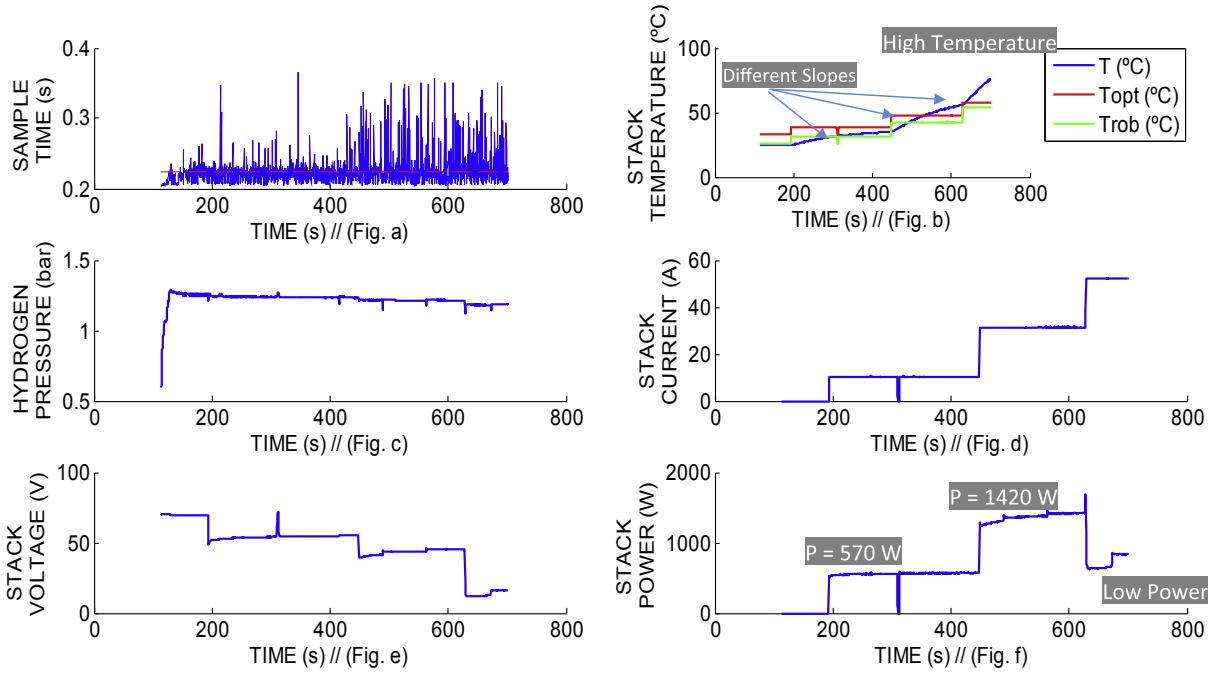

Fig. 8. AC-PEFC response for Configuration 1. From left to right and from top to bottom: (a)-Sample Time (s), (b)-Stack Temperature (ºC), (c)-Hydrogen Pressure (bar), (d)-Stack Current (A), (e)-Stack Voltage (V) and (f)-Stack Power (W).

temperature recommended by the manufacturer (Fig. 8b), we can deduce that during the first load steps, the stack temperature keeps between the established margins of robust and optimal temperature, recommended by manufacturer. However, the time interval that the stack temperature is between the robust and optimal temperature is decreasing when the load current is increasing.

Another test done over the developed AC-PEFC with the configuration 1 is a thermography analysis with a thermal imager model Testo 875-1i, with a range of −30 °C to +100 °C and ±2% accuracy). This analysis allows us to evaluate if the configuration under study is suitable or no as optimal Oxidant/Cooling subsystem. For this purpose, a thermography has been taken at the beginning of each load step. Authors have chosen the thermography as an alternative to use multiple thermocouples placed in the cooling channels by simplicity in the temperature diagnosis. In case of an air-cooled fuel cell as this, the cathode is designed with multiple channels for cooling, so this would lead to an extra-wired structure with one thermocouple located in each cooling channel. Additionally, thermocouples need to be in contact with the surface, but this is not easy in an 80-cells stack with 40 cooling channels each cell. Fig. 9a, b and 9c and Tables 3a, b and c show a no uniform temperature distribution.

At the beginning of the operating time interval (Fig. 9a) the stack temperature distribution is considerably no homogenous with a difference of 6.6 °C (Table 3a: M1 regarding M7) between the hottest and the coldest point. However, as the load current increases the difference of temperature between the hottest and the coldest point is more significant achieving at 13.8 °C (Table 3c: M4 regarding M10).

When the load current is 10 A (Table 3a), the higher temperature values can be found, in this order, in M1, M4, M2 and M5. In the case of 30 A (Table 3b), in M4, M5 and M1. Finally, for 50 A, in M4, M5, M1 and M2 (Table 3c). Notice that the hottest spots locations for configuration 1 are always on the upper left corner of the stack.

b)Configuration 2: Four fans covering the cathode area of the stack working two by two with flow control.

This second configuration aims to improve the AC-PEFC performance allowing to control the four fans. This will be done varying the fans speed taking into account the difference between the stack temperature and the optimal and robust temperature recommended by the manufacturer. For this configuration, the test bench is set up as in Fig. 2b.

Fig. 10 shows the flow chart of the operation with configuration 2. This is delimited by three stages. The experimental analysis starts calculating the difference between the stack temperature value and the optimal temperature at the operating point. Additionally, the variable called *LIMIT* presents the maximum value allowed for the difference between the stack temperature and the optimal temperature. In this case authors have established that $LIMIT = 3$. This value corresponds approximately to the difference.

$(Topt - Trob)/2$, when $I_{stack} = 0$. Then, in basis on the comparison between this temperatures difference and the allowable limit, the control system decides to activate one or two groups of fans and the speed they must rotate. The action carried out at each state is described as follow:

- State 0: the stack temperature value is well below the optimal temperature taking into account the established limit. Therefore, in this stage the stack needs to be warmed so fans will be switched off to avoid cooling the stack. The stack takes the air for breathing from the surrounding.
- State 1: the temperatures difference is inside the range of ±*LIMIT*. This means that the stack temperature is found between the accepted ranges recommended by the manufacturer. Therefore, it is necessary to keep the stack temperature inside this range. Therefore, GROUP 1 is put in working. The fan speed will be adjusted according to the expressions (3) and (4).

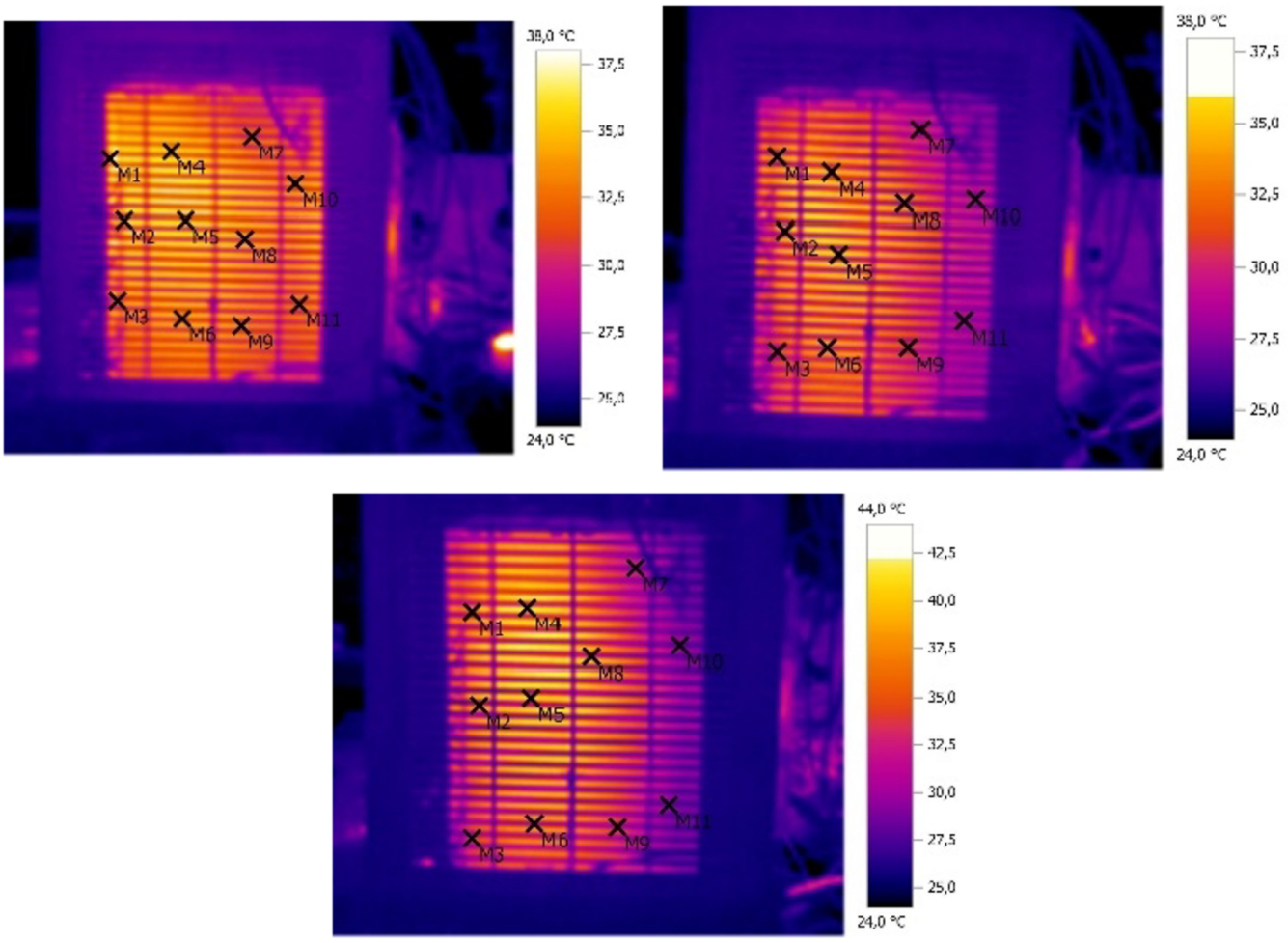

Fig. 9. a. Configuration 1: Thermography at 10 A. Fig. 9b. Configuration 1: Thermography at 30 A. Fig. 9c. Configuration 1: Thermography at 50 A.

Table 3a
Stack temperature points (Config. 1–10 A).

Point	Temp. (°C)	Emis	Ref. Temp. (°C)
M1	36.2 ± 2	0.94	25.0
M2	34.5 ± 2	0.94	25.0
M3	31.8 ± 2	0.94	25.0
M4	35.7 ± 2	0.94	25.0
M5	34.5 ± 2	0.94	25.0
M6	30.9 ± 2	0.94	25.0
M7	29.6 ± 2	0.94	25.0
M8	30.4 ± 2	0.94	25.0
M9	34.0 ± 2	0.94	25.0
M10	33.9 ± 2	0.94	25.0
M11	31.6 ± 2	0.94	25.0

Table 3b
Stack temperature points (Config. 1–30 A).

Point	Temp. (°C)	Emis	Ref. Temp. (°C)
M1	33.0 ± 2	0.94	25.0
M2	31.5 ± 2	0.94	25.0
M3	31.7 ± 2	0.94	25.0
M4	35.2 ± 2	0.94	25.0
M5	34.8 ± 2	0.94	25.0
M6	29.1 ± 2	0.94	25.0
M7	30.3 ± 2	0.94	25.0
M8	27.8 ± 2	0.94	25.0
M9	30.7 ± 2	0.94	25.0
M10	29.6 ± 2	0.94	25.0
M11	27.8 ± 2	0.94	25.0

$$DIF = (DIF - 2\ .LIMIT)K_1 \tag{3}$$

$$Fan_{Speed}(\%) = 100\ \frac{DIF}{2\ .LIMIT} + 50 \tag{4}$$

- State 2: the temperatures difference is far above the defined *LIMIT*. This means than the stack temperature is higher than the optimal temperature taking into account the *LIMIT*. Therefore, both fans groups (GROUP 1 and GROUP 2) must to be activated.

In this state, the fan speed will be adjusted according to the expressions (5) and (6).

$$DIF = DIF\ .\ K_2 \tag{5}$$

$$Fan_{Speed}(\%) = 100\frac{DIF}{2\ .\ LIMIT} + 50 \tag{6}$$

where $K_1 = 1$ and $K_2 = 2$, are variables related to how much the error should be increased and therefore how quickly we expect the control acts. Authors in basis on system response have chosen these constant values.

Table 3c
Stack temperature points (Config. 1–50 A).

Point	Temp. (°C)	Emis	Ref. Temp. (°C)
M1	35.2 ± 2	0.94	25.0
M2	35.0 ± 2	0.94	25.0
M3	34.0 ± 2	0.94	25.0
M4	41.5 ± 2	0.94	25.0
M5	40.9 ± 2	0.94	25.0
M6	29.9 ± 2	0.94	25.0
M7	28.6 ± 2	0.94	25.0
M8	31.6 ± 2	0.94	25.0
M9	30.4 ± 2	0.94	25.0
M10	27.7 ± 2	0.94	25.0
M11	28.1 ± 2	0.94	25.0

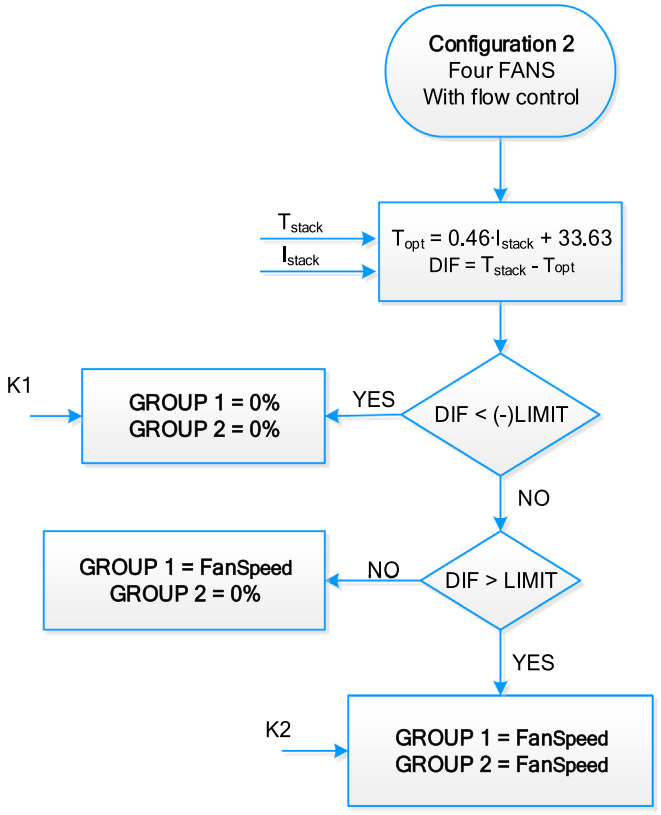

Fig. 10. Flow chart of configuration 2: Four fans working two by two with flow control.

Like in the Configuration 1, the study of the dynamic stack behaviour will be done using a multi steps load profile (10A–30A – 50A).

The fuel cell response is going to be analysed attending to stack temperature, voltage, current, power, hydrogen pressure and a multi steps load profile (10 A–30 A – 50 A) is used. From Fig. 11b, we can see how the stack temperature changes when no current is demanded by the load; this is because the previous study was done before this one, so the stack is still warmed. Therefore, we can appreciate how the configuration is capable of decreasing the stack temperature from 60 °C (due to the previous test) up to 30 °C, which is the optimal temperature for the first load current step. The time when the load changes can be guessed perfectly over the stack temperature response. Moreover, like in the previous configuration, it is noticed that the stack temperature slope does not depend on the step amplitude difference but on the actual current value at this time. That is for the step between 10 A–30A, the amplitude step (20 A) is similar to the step amplitude between 30 A–50 A. However, the temperature slope and curvature are different. The curvature slopes are 0.05 and 0.1 for 30 and 50 A, respectively.

Another observation we can do about Fig. 11 is the stack electrical performance: attending to stack voltage response, when load demand rises up to 50 A, the stack voltage does not drop and the power supplied reaches above 2000 W avoiding air-starvation problem. Therefore, for this configuration it does not seem to be air supply problems.

Additionally, comparing the stack temperature with the optimal and robust temperature recommended by the manufacturer (Fig. 11b), we can deduce that the stack temperature is controlled between the robust and optimal temperature during almost all the load demand. Just in the last load step, the stack temperature is slightly above the range recommended by the manufacturer.

Similarly to configuration 1, now with configuration 2 a thermography analysis has been done as well, in order to evaluate if the configuration under study is suitable or not as optimal Oxidant/Cooling subsystem. For this purpose, a thermography has been taken at the beginning of each load step. Fig. 12a, b and c; and Tables 4a, b and c show a better uniform temperature distribution regarding configuration 1.

In the first operating time interval (Fig. 12a) the stack temperature distribution is significantly no homogenous with a difference of 5.6 °C (Table 4a: M1 regarding M11) between the hottest and the coldest point. However, as the load current increases, the difference of temperature between the hottest and coldest point increases, achieving at 10.3 °C (Table 4b: M4 regarding M10) and 18.1 °C (Table 4c: M4 regarding M9).

When the load current is 10 A (Table 4a), the higher temperature values can be found, in this order, in M1, M5, M2 and M6. In the case of 30 A (Table 4b), in M4, M1, M6 and M2. Finally, for 50 A, in M4, M1 and M5 (Table 4c). Again, note that the hottest spots locations for configuration 2 are always on the left side of the stack.

c) Configuration 3: One single speed controlled fan.

In this case, the control logic results from a combination of the two previous control diagrams. Similarly, it calculates the difference between the stack temperature and the optimal temperature at the operating point and establishes the LIMIT value (in this third case authors have established that LIMIT = 3).

The action carried out at each state is described as follow (Fig. 13):

- State 0: when the difference between the stack temperature and the optimal temperature is lower that (−) LIMIT, the stack far to be cooled it needs to be warmed. An excess of cooling could originate flooding of the membrane, affecting the stack performance. In configuration 2 all the fans were switched off, but in this case the fan is kept at its minimum controllable speed (700 min^{-1}), which is 15% of the minimum speed according to datasheet [31], with the aim to avoid the air starvation problem, supplying the minimum amount of air needed by the stack for breathing.
- State 1: when the temperatures difference is inside the range of ± LIMIT, the stack temperature is found between the accepted ranges. Then, with the aim to keep the stack temperature inside this range, the fan speed is adjusted according to expressions (7).

$$Fan_{Speed}(\%) = 100 \ \frac{DIF}{2 \ . \ LIMIT} + 50 \qquad (7)$$

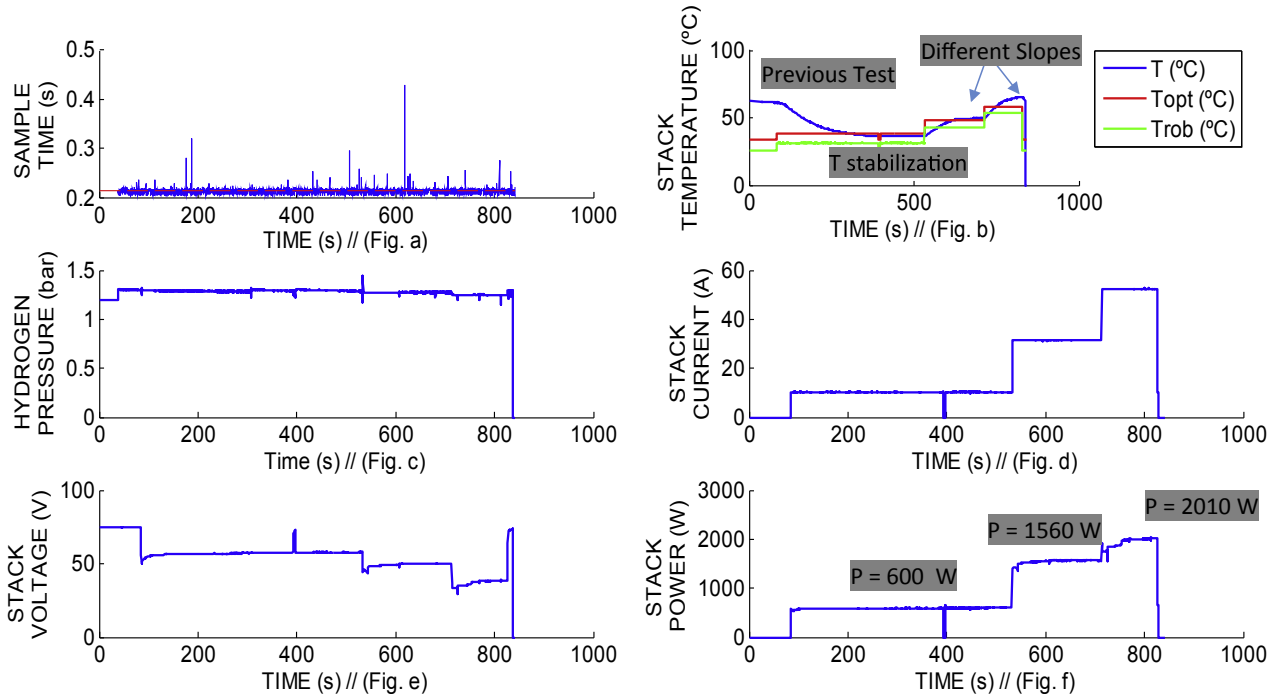

Fig. 11. AC-PEFC for Configuration 2. From left to right and from top to bottom: (a)-Sample Time (s), (a)-Stack Temperature (°C), (c)-Hydrogen Pressure (bar), (d)-Stack Current (A), (e)-Stack Voltage (V) and (f)-Stack Power (W).

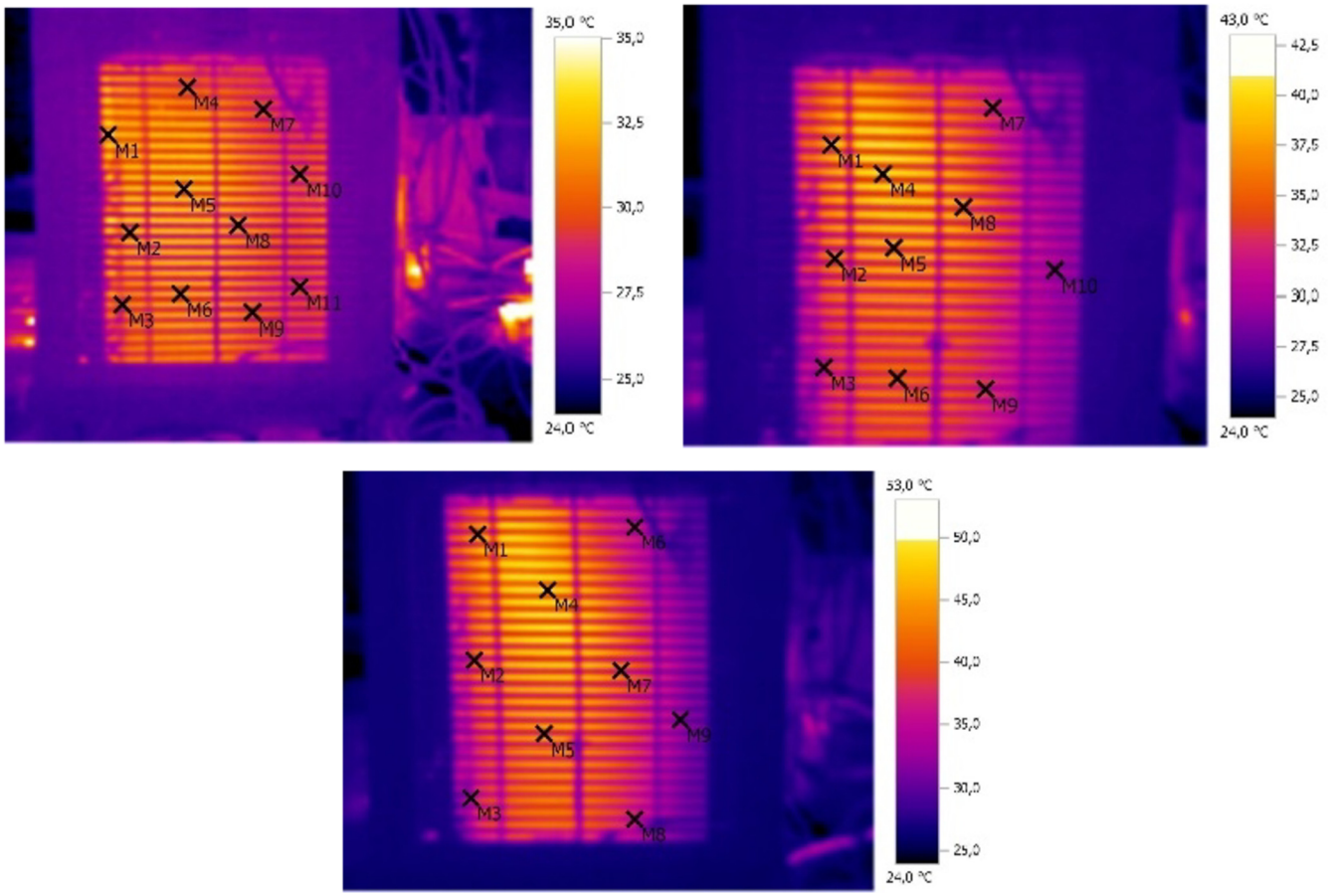

Fig. 12. a. Configuration 2: Thermography at 10 A. Fig. 12b. Configuration 2: Thermography at 30 A. Fig. 12c. Configuration 2: Thermography at 50 A.

Table 4a
Stack temperature points (Config. 2–10 A).

Point	Temp. (°C)	Emis	Ref. Temp. (°C)
M1	33.6 ± 2	0.94	26.5
M2	32.3 ± 2	0.94	26.5
M3	30.3 ± 2	0.94	26.5
M4	29.4 ± 2	0.94	26.5
M5	33.2 ± 2	0.94	26.5
M6	32.3 ± 2	0.94	26.5
M7	28.3 ± 2	0.94	26.5
M8	28.3 ± 2	0.94	26.5
M9	29.7 ± 2	0.94	26.5
M10	28.3 ± 2	0.94	26.5
M11	28.0 ± 2	0.94	26.5

Table 4b
Stack temperature points (Config. 2–30 A).

Point	Temp. (°C)	Emis	Ref. Temp. (°C)
M1	38.3 ± 2	0.94	26.5
M2	34.7 ± 2	0.94	26.5
M3	33.0 ± 2	0.94	26.5
M4	40.2 ± 2	0.94	26.5
M5	33.7 ± 2	0.94	26.5
M6	34.8 ± 2	0.94	26.5
M7	32.0 ± 2	0.94	26.5
M8	33.2 ± 2	0.94	26.5
M9	30.9 ± 2	0.94	26.5
M10	29.9 ± 2	0.94	26.5

Table 4c
Stack temperature points (Config. 2–50 A).

Point	Temp. (°C)	Emis	Ref. Temp. (°C)
M1	39.8 ± 2	0.94	26.5
M2	36.4 ± 2	0.94	26.5
M3	34.1 ± 2	0.94	26.5
M4	49.2 ± 2	0.94	26.5
M5	37.5 ± 2	0.94	26.5
M6	36.6 ± 2	0.94	26.5
M7	36.2 ± 2	0.94	26.5
M8	34.4 ± 2	0.94	26.5
M9	31.1 ± 2	0.94	26.5

- Stage 2: finally, when the temperatures difference is far above the defined LIMIT, the fan must rotate at its maximum speed (5500 min^{-1}) to guarantee both the air breathing of the stack and the temperature control.

Additionally to the previous control stages, it is necessary to point out that the control strategy has to be also based in the following: in case of stack model used in this work, the stoichiometric rate of the stack recommended by manufacturer varies between 50 and 200. Due to this range is excessively wide, it can happen that working inside the stoichiometric range, the stack performance was long from the optimal. Based on this, authors propose the control diagram for configuration 3 with the aim to accomplish with the restrictions related to stoichiometric range at time that it pursues to maintain the stack temperature between the recommended values. This condition of stack temperature is more restrictive than the air stoichiometry criterion. In this case, the difference between the optimal and robust temperature is not higher than 7 °C, so the oxidant/cooling subsystem must be controlled with the aim to guarantee this narrow operating temperature margin.

The experimental results obtained for this configuration are shown in Fig. 14. Like in the previous configurations, the study of

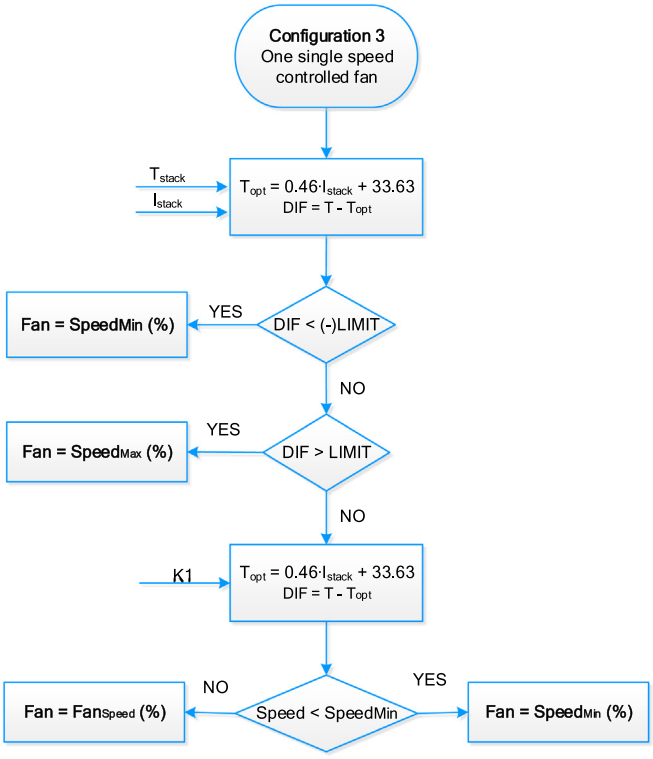

Fig. 13. Flow chart of configuration 3: One single speed controlled fan.

the dynamic stack behaviour will be done using a multi steps load profile (10A–30A– 50A). From Fig. 14, we can point out how the stack temperature remains stabilized when the load demands no current; this is because the stack is cold. The time when the load changes can be guessed perfectly over the stack temperature response. Moreover, for all load currents, it can be pointed out that the stack temperature is between the recommend range (optimal and robust temperature values) and it keeps stabilized in the same way that for 0 A. Unlike to previous configurations, where the stack temperature slope did not depend on the step amplitude difference but on the actual current value, now the temperature slope and curvature are identical at the step between 10 A–30A (amplitude step of 20 A) and at the step between 30 A–50 A.

Another observation we can appreciate over Fig. 14 is the stack electrical performance: attending to stack power response, when load demand rises up to 50 A, the stack power does not drop abruptly like it happened in configuration 1 (remember Fig. 8), but it achieves more than 2500 W.

Regarding the thermography analysis that has been done to evaluate if the configuration under study is suitable or not as optimal Oxidant/Cooling subsystem, in this case like in the previous ones, a thermography has been taken at the beginning of each load step. Fig. 15a, b and c, and Tables 5a, b and c, show uniform temperature distribution. In the first operating time interval (Figure 15a) the stack temperature distribution is practically homogenous with a difference of 0.8 °C (Table 5a: M5 regarding M6) between the hottest and the coldest point. As the load current increases, the difference of temperature between the hottest and the coldest point increases slightly, achieving at 1.1 °C (Table 5b: M5 regarding M3) and 1.4 °C (Table 5c: M5 regarding M3).

Regarding the results obtained up to now, we can have some relevant data to foresee what configuration fulfils the six requirements that the oxidant/cooling system must guarantee. Just as a reminder, they were (Fig. 1): 1) To be able to cool the stack

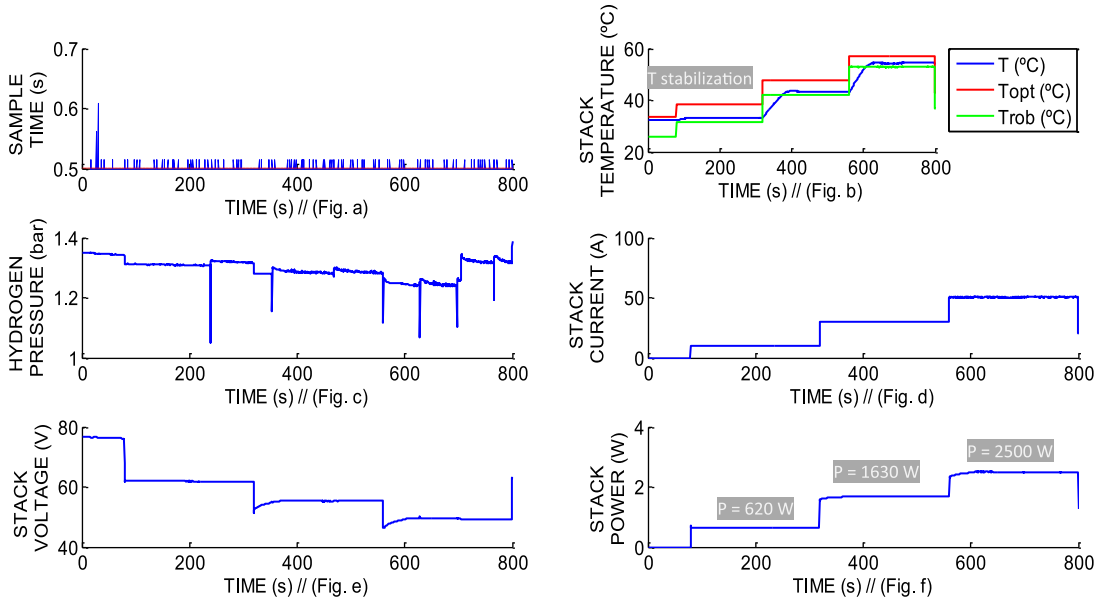

Fig. 14. AC-PEFC for Configuration 3. From left to right and from top to bottom: (a)-Sample Time (s), (b)-Stack Temperature (ºC), (c)-Hydrogen Pressure (bar), (d)-Stack Current (A), (e)-Stack Voltage (V) and (f)-Stack Power (W).

homogeneously, 2) To provide sufficient airflow range to control the PEFC temperature under a range of power and room/coolant air temperature, 3) To place the stack at optimum temperature, 4) To reduce the auxiliary power consumption, 5) To do all this within a certain sized box, and finally but not least 6) To do it cost effectively.

Based on the tests performed, it is clear that the only configuration able to meet the requirements is the configuration 3. However, we still have to prove that it provides sufficient airflow range to control the PEFC temperature, under a range of power and room/coolant air temperature. The previous test has been carried out

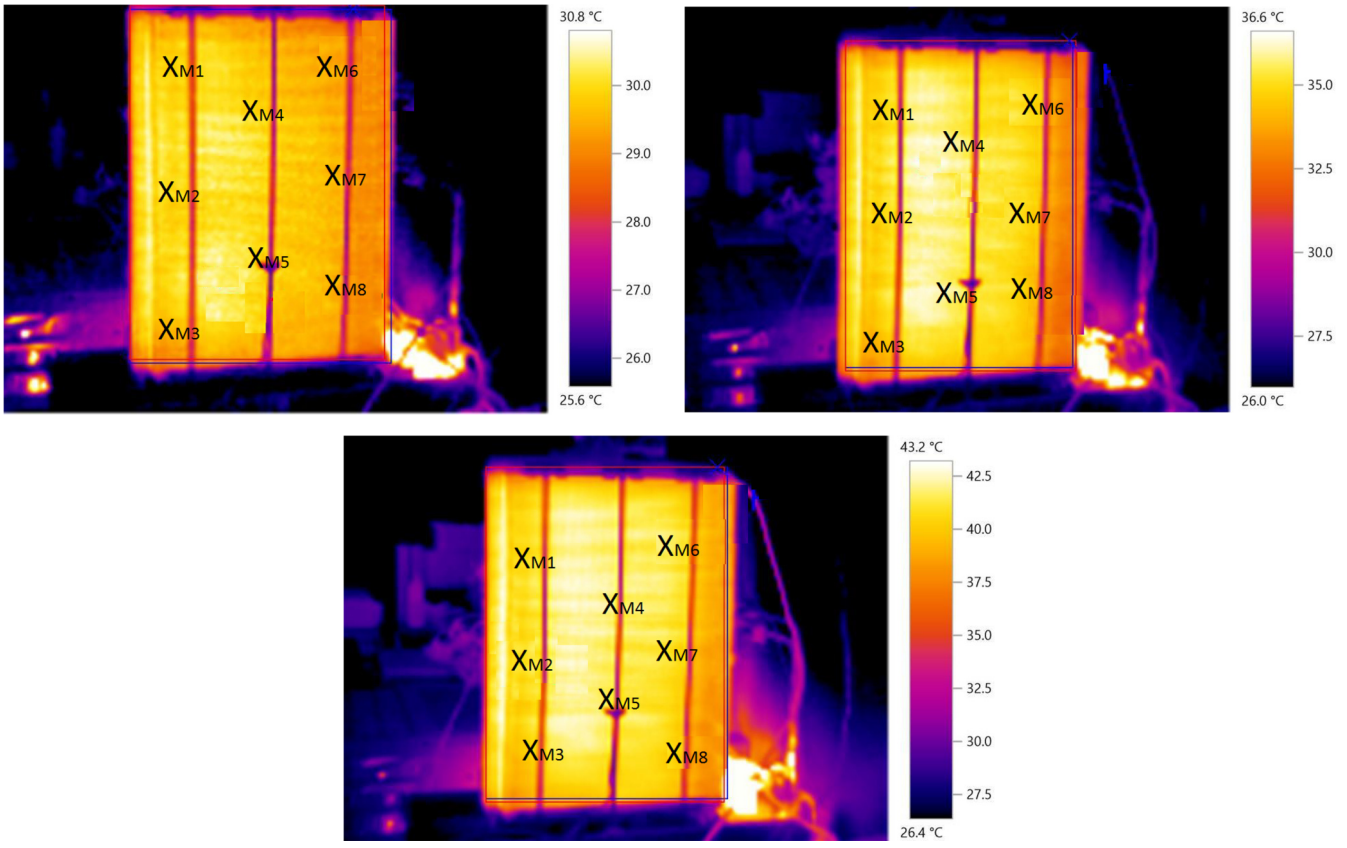

Fig. 15. a. Configuration 3: Thermography at 10 A. Fig. 15b. Configuration 3: Thermography at 30 A. Fig. 15c. Configuration 3: Thermography at 50 A.

Table 5a
Stack temperature points (Config. 3–10 A).

Point	Temp. (ºC)	Emis	Ref. Temp. (ºC)
M1	30.2 ± 2	0.94	23
M2	30.5 ± 2	0.94	23
M3	30.1 ± 2	0.94	23
M4	30.6 ± 2	0.94	23
M5	30.8 ± 2	0.94	23
M6	30.0 ± 2	0.94	23
M7	30.7 ± 2	0.94	23
M8	30.2 ± 2	0.94	23

Table 5b
Stack temperature points (Config. 3–30 A).

Point	Temp. (ºC)	Emis	Ref. Temp. (ºC)
M1	35.9 ± 2	0.94	23
M2	36.5 ± 2	0.94	23
M3	35.7 ± 2	0.94	23
M4	36.6 ± 2	0.94	23
M5	36.8 ± 2	0.94	23
M6	36.0 ± 2	0.94	23
M7	36.7 ± 2	0.94	23
M8	36.3 ± 2	0.94	23

Table 5c
Stack temperature points (Config. 3–50 A).

Point	Temp. (ºC)	Emis	Ref. Temp. (ºC)
M1	42.2 ± 2	0.94	23
M2	43.1 ± 2	0.94	23
M3	42.0 ± 2	0.94	23
M4	43.2 ± 2	0.94	23
M5	43.4 ± 2	0.94	23
M6	42.6 ± 2	0.94	23
M7	43.3 ± 2	0.94	23
M8	42.1 ± 2	0.94	23

with a fix room temperature of 23 °C and an initial stack temperature of 33 °C.

Then, with the aim to probe that the developed oxidant/cooling subsystem provides sufficient air in a room temperature range, a last test will be done over configuration 3. Now the room temperature has been lowered to 13 °C, which logically brings a significant drop in stack temperature. The results of this new test are shown in Fig. 16.

Regarding Fig. 16, we can observe that stack reaches the temperature recommended by the manufacturer at the end of the first step, due to its low starting temperature. In fact, as you can see in Fig. 16b, it takes about 6 min for the temperature to be inside the window (*Top* − *Trob*). From here, the behaviour of the stack temperature is becoming more and more suitable. Nevertheless, in basis on power output, the stack performance is not affected. Then we can advance that the stack can provide the design power even when its starting temperature is below the design temperature.

Regarding the thermographies (Figures 17a, b and c; and Tables 6a, b and c, at the beginning the difference of Tables 5a and 6a, is practically the same as the drop in room temperature. This is, around 10 °C. However, as the stack is working, the gap is coming reduced, and at the end of the test, it is only around 5 °C.

5. Discussion

In the red-ox reaction that takes place in a fuel cell, the hydrogen energy is transformed into electrical power and heat. A stack temperature control non-optimized will lead to a fuel cell where the most of the hydrogen energy is converted into heat, resulting an inefficient system. However, a temperature control in which the aims is not only to adjust the air stoichiometry but to fix the stack temperature between the recommended ranges, provides a better fuel cell efficiency: with the same hydrogen consumption, it supplies higher electrical power.

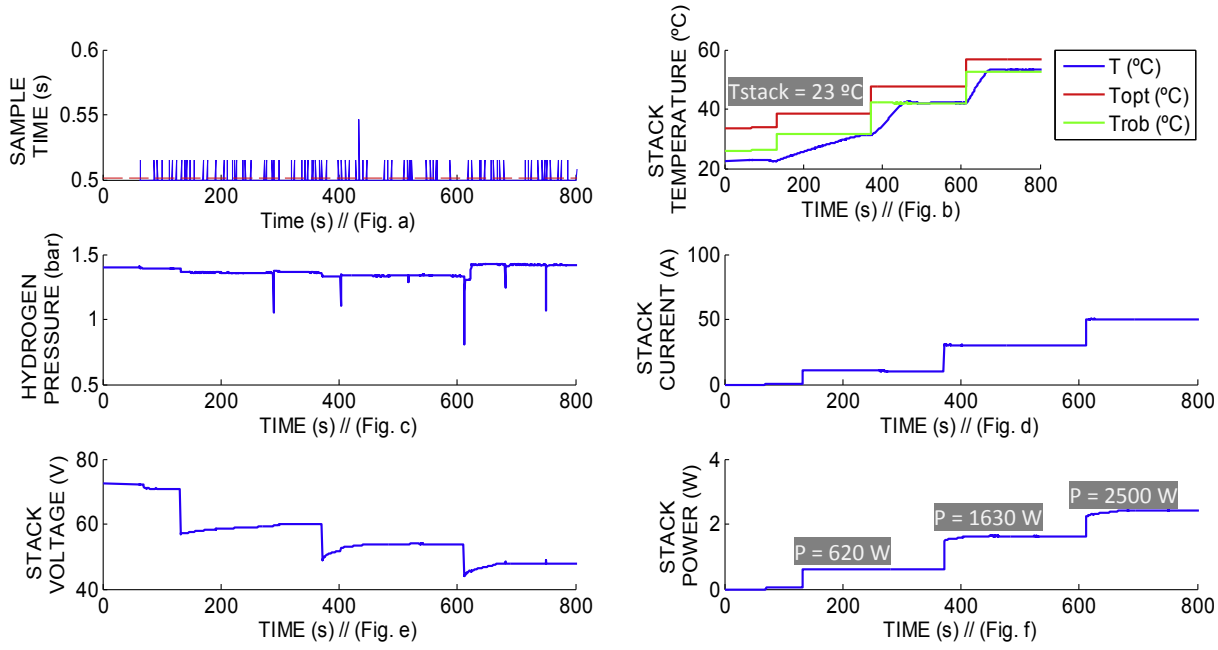

Fig. 16. AC-PEFC for Configuration 3: Test 2. From left to right and from top to bottom: (a)-Sample Time (s), (b)-Stack Temperature (ºC), (c)-Hydrogen Pressure (bar), (d)-Stack Current (A), (e)-Stack Voltage (V) and (f)-Stack Power (W).

Table 6a
Stack temperature points (Config. 3–10 A).

Point	Temp. (°C)	Emis	Ref. Temp. (°C)
M1	20.3 ± 2	0.94	13
M2	20.1 ± 2	0.94	13
M3	20.0 ± 2	0.94	13
M4	19.8 ± 2	0.94	13
M5	20.2 ± 2	0.94	13
M6	19.1 ± 2	0.94	13
M7	19.0 ± 2	0.94	13
M8	20.3 ± 2	0.94	13
M9	19.7 ± 2	0.94	13
M10	19.5 ± 2	0.94	13

Table 6b
Stack temperature points (Config. 3–30 A).

Point	Temp. (°C)	Emis	Ref. Temp. (°C)
M1	30.8 ± 2	0.94	13
M2	31.5 ± 2	0.94	13
M3	30.0 ± 2	0.94	13
M4	30.6 ± 2	0.94	13
M5	32.6 ± 2	0.94	13
M6	31.9 ± 2	0.94	13
M7	30.4 ± 2	0.94	13
M8	32.0 ± 2	0.94	13
M9	30.0 ± 2	0.94	13
M10	23.7 ± 2	0.94	13

Table 6c
Stack temperature points (Config. 3–50 A).

Point	Temp. (°C)	Emis	Ref. Temp. (°C)
M1	36.5 ± 2	0.94	13
M2	37.6 ± 2	0.94	13
M3	36.5 ± 2	0.94	13
M4	36.1 ± 2	0.94	13
M5	38.6 ± 2	0.94	13
M6	37.9 ± 2	0.94	13
M7	35.8 ± 2	0.94	13
M8	37.0 ± 2	0.94	13
M9	36.6 ± 2	0.94	13
M10	29.8 ± 2	0.94	13

In this work, for developed configurations 1 and 2, with 4 fans (Fig. 2b), authors have proposed these designs in basis on stack's manufacturer recommendations based on a polycarbonate enclosure around the stack. This structure serves as stand to support four fans that cover the area of the stack cathode. Regarding configuration 3 with only a fan (Fig. 2c), the design aim of the authors has been to improve the air breathing of the stack and its temperature distribution over the cathode. This third configuration tries to sort out the problem observed in configurations 1 and 2: the air follows preferential paths surrounding the stack instead of crossing it for its cooling. In this sense, authors have proposed a design consisting on a speed controllable fan, which is inserted in a cone-shaped hopper built to facilitate the air blow through the stack and avoiding preferential paths of the airflow.

In configuration 1 the fans operate in ON/OFF mode. In configuration 2, the fans are controlled based on the difference between the stack temperature and the optimal temperature recommended by manufacturer. In configuration 3, the single fan works with variable speed, under a control law whose purpose is to maintain the stack temperature within the window of suitable operating temperatures of the stack. Someone might wonder why the authors have not designed a controller, such as a PID for example that can track the optimum temperature (it would have even been easier than the proposed solution). The answer is that the heating process is not controlled, it depends on the power requested to the stack at any time, and the cooling process, based on ventilation, does not allow to follow a set point exactly; consequently, it is better, more practical and efficient, to work in a window of allowed values.

The three proposed configurations have been tested under the same conditions and load profile. The goal to compare proposed configurations is to verify the fulfilment of the six design challenges proposed at the beginning of the work. These challenges are:

1) To be able to cool the stack homogeneously.
2) To provide sufficient airflow range to control the PEFC temperature, under a range of power and room/coolant air temperature.
3) To place the stack at optimum temperature.
4) To reduce the auxiliary power consumption.
5) To do all this within a certain sized box, and
6) To do it cost effectively.

Analysing the experimental results, we can observe that in configuration 1 (Fig. 8), the stack temperature does not change when no current is demanded by the load. Next, stack temperature starts to increase as load current gets higher. The time when the load changes can be guessed perfectly over the stack temperature response. Moreover, we can notice, the stack temperature slope does not depend on the step amplitude difference but on the actual current value at this time. That is, for the step between 10 A–30 A, the amplitude step (20 A) is similar to the step between 30 A–50 A. However, the temperature slopes and curvatures are different. The curvature slopes are 0.1 °C/A at 10 A, 0.05 °C/A at 30 A and 0.4 for 50 A.

Another observation we can do over Fig. 8 is the electrical performance of the fuel cell. Attending to voltage response, when load demand rises up to 50 A, the stack voltage drops significantly reducing the power supplied by the stack below 1000 W. Attending to the real AC-PEFC implementation and the BoP configuration

Table 7
Analysis of Oxidant/Cooling system parameters.

Configuration		Air required $\boldsymbol{Air_{stack}}$ (m^3/h)	Heat Generated $\boldsymbol{Q_{stack\_\_heat}}$ (W)	Air Volume needed for cooling $\boldsymbol{\dot{V}_s}$·(m^3/h) [λ[a]]	Total Air Pressure drop $\boldsymbol{\Delta P_{total}}$(Pa)	Fan operating point
# 1	10 A	0.79	470	132.73 [166.59]	44.43	OFF: 0
	30 A	2.39	1560	179.75 [75.19}	52.69	ON: 5500 rpm
	50 A	3.98	4500	270.06 [67.78]	69.43	
# 2	10 A	0.79	450	112.72 [141.41]	41.40	0–5500 rpm
	30 A	2.39	1505.7	177.04 [74.06]	52.22	According to control
	50 A	3.98	2990	215.33 [54.04]	59.58	algorithm (Fig. 10)
# 3	10 A	0.79	380	109.46 [137.38]	40.84	700–5500 rpm
	30 A	2.39	1370	164.44 [68.79]	50.18	According to control
	50 A	3.98	2500	211.81 [53.16]	58.53	algorithm (Fig. 13)

[a] λ is the stoichiometric rate and it is defined as:λ = air flow needed for cooling/air flow required for oxidant reaction.

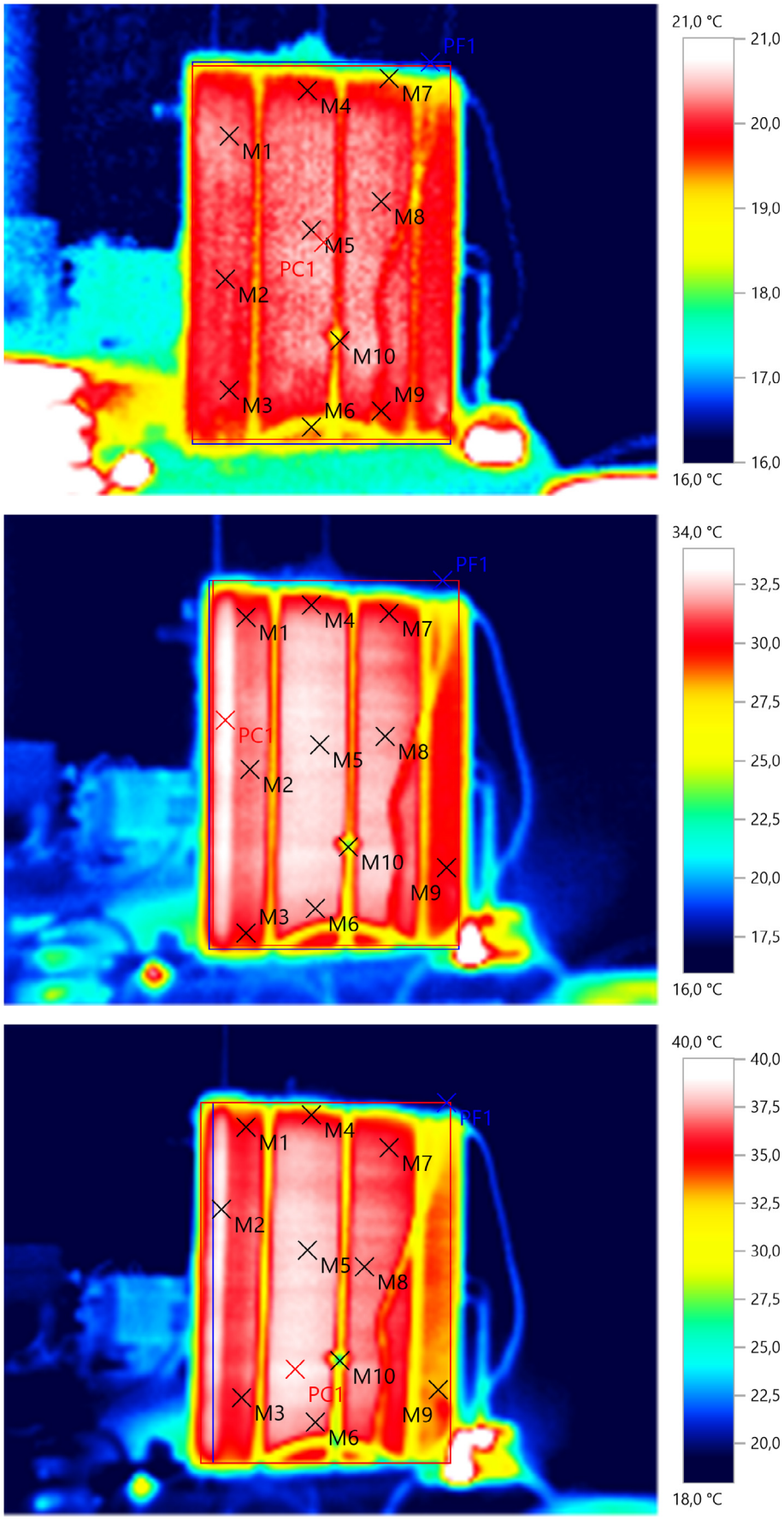

Fig. 17. a. Configuration 3. Test 2: Thermography at 10 A. Fig. 17b. Configuration 3. Test 2: Thermography at 30 A. Fig. 17c. Configuration 3. Test 2: Thermography at 50 A.

(Fig. 2), two reasons could be the origin of this: a wrong hydrogen supply or an inefficient oxidant supply system. They are the only two agents involved in the stack red-ox reaction. Attending to hydrogen pressure response (Fig. 8c), it has been kept fixed along the whole test so this leads us to think the high temperature achieved by the stack (Fig. 8b) is due to an improper air-breathing and the oxidant/cooling system is inefficient. Remember that the air-starvation problem can affect the electrical resistivity of the membrane because the membrane is very dry to allow passing ions across itself.

Based on the above, configuration 1 is an inefficient Oxidant/Cooling subsystem. The stack temperature increases continually (Fig. 8b) because the Oxidant/Cooling subsystem is not capable of maintaining the stack temperature value between the recommended ranges. Therefore, the system requires a better control over the fans to adjust properly the stack temperature as well as to supply the air needed for breathing. Additionally, there is a clear air-starvation problem, reducing considerably the fuel cell efficiency. The thermography images taken along the load profile (Fig. 9a, a and 9c) show clearly how the airflow surrounds the stack following preferential paths because the hottest spots locations are always (regardless of the power demanded) on the upper left corner of the stack (see also values on Tables 3a, b and c). So, a diagonal-shape operating mode for fans activated two by two is not recommended.

Regarding configuration 2, it solves the air-starvation problem presented by configuration 1. Besides, it shows a better stack temperature response (Fig. 11). It increases continually as load current rises and it is closer to the optimal temperature (Fig. 11b) than configuration 1, but most of the time it is still outside. Regarding the fuel cell efficiency, this is better than in previous configuration. However, the stack temperature distribution is still no uniform; note that the hottest spots locations for configuration 2 are always on the left side of the stack (please, see Fig. 12a, b and 12c; and Tables 4a, b and c). In fact, the no-uniformity in the stack temperature is even more noticeable than in configuration 1. This can be appreciated in the thermographies at different load current values. Table 4c shows that there is a difference greater than 18 °C between the hottest and the coldest point at the same time in the same stack.

Finally, the last proposed configuration avoids the preferential paths because the cone-shaped hopper is totally adapted to the stack avoiding the space between the stack and the structure for the air flow. Therefore, the airflow is forced to cross the stack in order to cool it. In this case, experimental results show the stack temperature is fairly well adjusted to optimal temperature, guaranteeing both the stack oxygenation and cooling (please, see Figs. 14 and 15, and Tables 5a, b and C). That is, both air-starvation and no-homogeneous cooling problems from configurations 1 and 2 are solved. As consequence, this design guarantees both the more proper air breathing subsystem for the stack and the best fuel cell efficiency. Additionally, thermography images demonstrate the best temperature distribution is around the stack cathode area.

Up to now, with the tests done over configurations 1, 2 and 3 we can advance what configuration best fulfils the six requirements that the oxidant/cooling system must guarantee (see Fig. 1). The last question that has been addressed in this paper is the oxidant/cooling subsystem capability. As it was introduced, one of the requirements is to provide enough airflow under different power outputs and room temperatures. On the other hand, as it is demonstrated in Ref. [15], the airflow rate needs are higher for stack cooling than for oxygenation. Therefore, if the stack cooling is guaranteed, the stack oxygenation will be too. In this regard, the cooling airflow rate depends on the difference between the stack and air temperature; higher difference, higher airflow needs. Then, the fan selection [15] was done considering the highest temperature the stack could achieve (66 °C at nominal power). Then, the first test applied over configuration 3 confirms the design is suitable for supplying enough airflow to oxygenate and cool the stack at a certain room temperature. The second test completes the first one showing the proper stack oxygenation and cooling for a room temperature range. Regarding this (please see Figs. 16 and 17 and Table 6a, b, c), it is clear that air starvation (deficiency of configuration 1) and high stack temperatures (deficiency of configurations 1 and 2) have more negative effect on the stack performance than a cool starting. In a real application, in case the user desires to start working inside the temperature range, it is advisable to wait a few minutes to warm the stack.

The effects of a proper design of the Oxidant/Cooling subsystem can be observed directly over the stack performance. Then, if the stack is operated at temperatures above optimal one, the membrane will dry out and become more electrically resistive, reducing

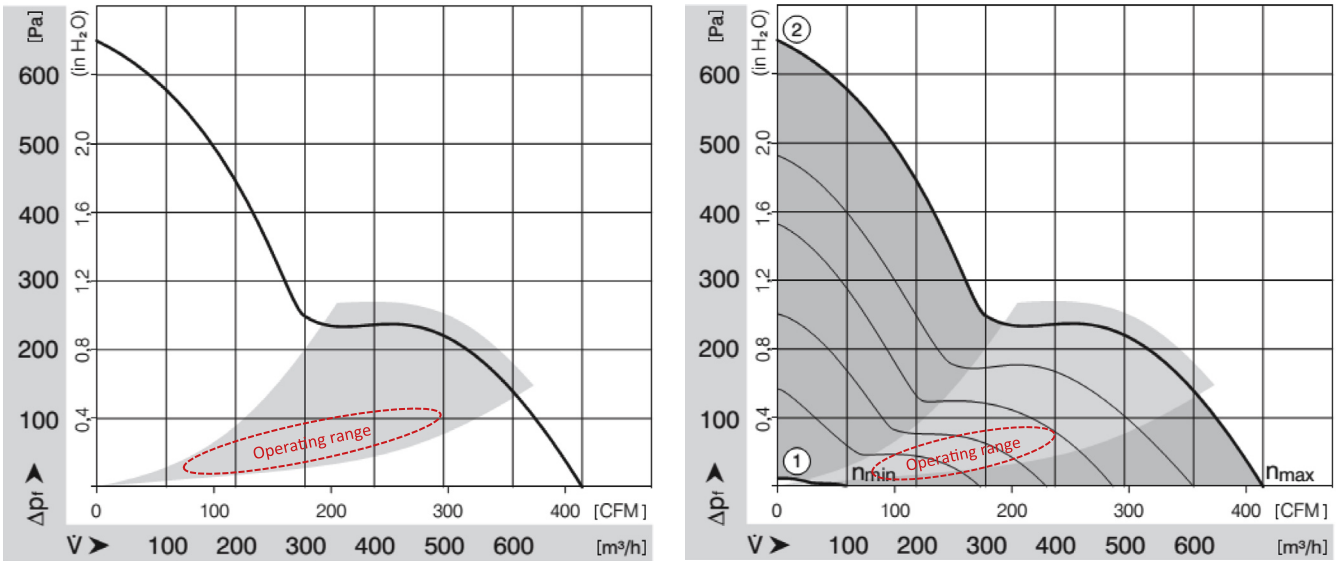

Fig. 18. a. Air chart for fan model Embpast-6224TD (Configuration 1 and 2). Fig. 18bAir chart for fan model Embpast-6224TD (Configuration 3).

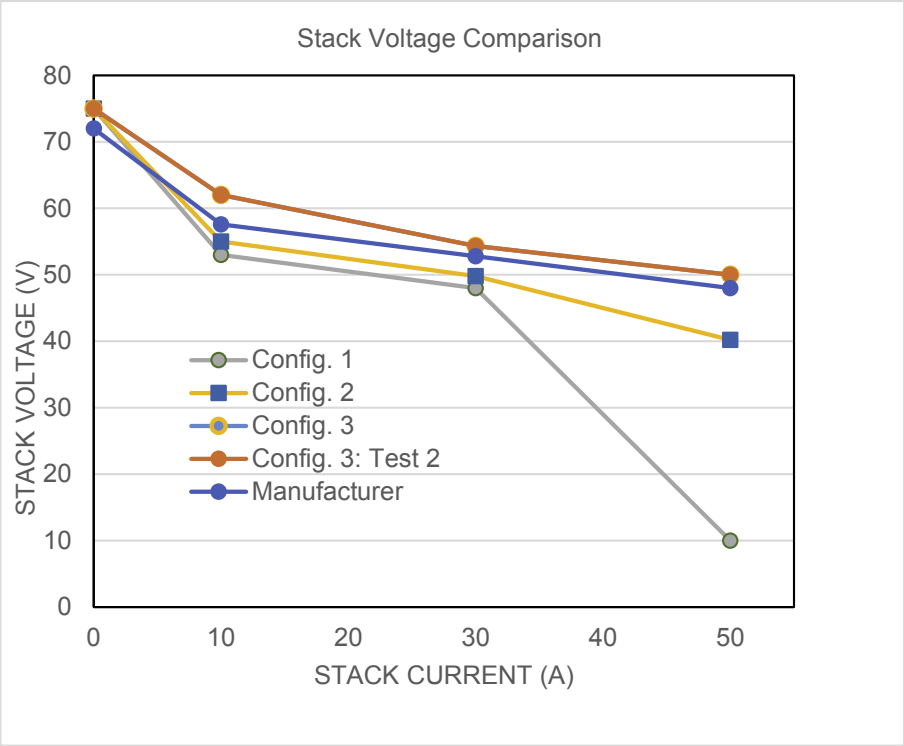

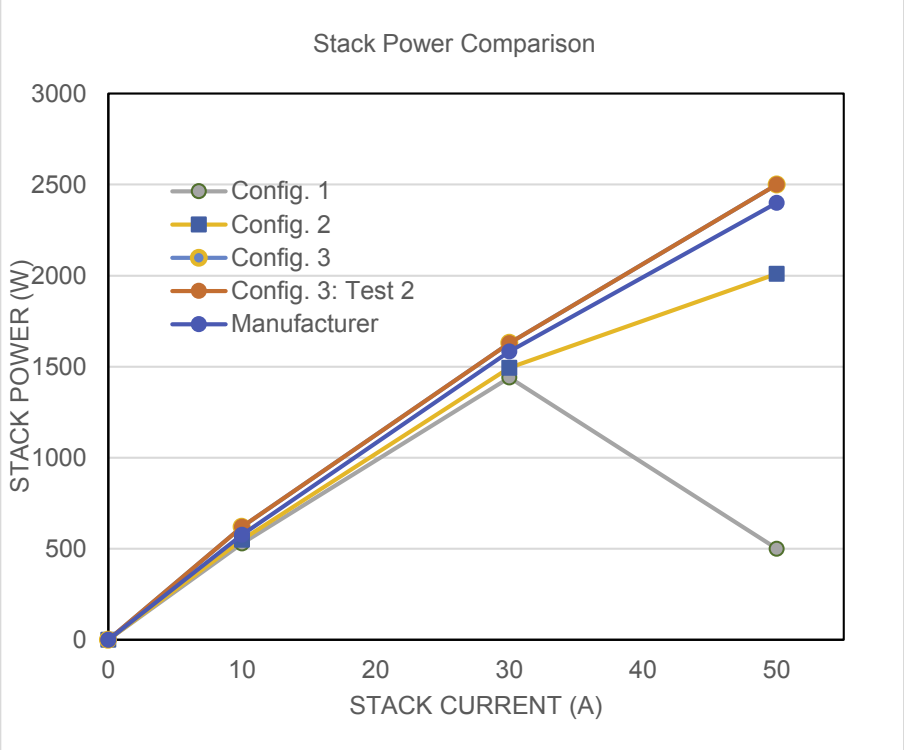

Fig. 19. a. Stack Voltage Comparison. Figure 19b. Stack Power Comparison. Fig. 19c. Stack Temperature Comparison.

the stack performance. This is the case of configurations 1 and 2. Even at extreme temperatures, the membrane can become damaged, resulting in irreversible performance losses. Specifically, in configuration 1 due to an improper air-breathing and inefficient oxidant/cooling system, stack suffers air-starvation problem. This provokes there is no sufficient air for the redox reaction in the membrane (oxygen and hydrogen mix to form electricity and water) and, consequently the voltage will decrease significantly, decreasing too the power provided by the stack.

By contrast, if the stack is operated at temperatures well below optimal value, the membrane will be over-humidified, resulting in the presence of liquid water in the cells. Too much water can cause

anode flooding, where the water blocks reactants from reaching the catalyst layer. This can also cause irreversible performance loss though localized fuel starvation and cell reversals. For this reason, the temperature control system developed in configuration 3 keeps the stack temperature very close to the optimum value. That is, in configuration 3, the one that shows the best stack performance, there are no situations of air-starvation, nor dry or flooded membrane.

Paying attention to thermographies we can observe configuration 1 point out clearly that the airflow surrounds the stack following preferential paths because the hottest spots appear on the upper left corner of the stack. With regard to the difference between the coldest and hottest point at highest current value (50A), it has been justified than it can achieve more than 13 °C, respect to the value 73 °C, given by the temperature sensor provided into the stack by the manufacturer. Therefore, the stack temperature distribution in configuration 1 is no uniform at all.

Regarding thermographies obtained from configuration 2, they show how the stack temperature distribution is still no uniform. In this case, the hottest points also appears on the upper left side of the stack, very similar to configuration 1. Moreover, the difference between the coldest and hottest point at highest current value (50A), is worse than in the first configuration, increasing up to 18 °C taking as reference the value of 65 °C given by the temperature sensor.

In the last configuration, the third, thermography images point out that the best temperature distribution is around the stack cathode area. In this case, temperature distribution is clearly homogeneous in the two cases (configuration 3-Test 1 and configuration 1-Test 2. The difference between the coldest and hottest point is 1.4 °C, while the value offered by the temperature sensor is 65 °C. Then, we can conclude that the best configuration, besides it involves a more complex control into the fan, is configuration 3. It guarantees the best air breathing and cooling into the stack, homogenous temperature distribution and the best stack performance.

Once the three proposed configurations have been discussed separately, now we are going to compare the main factors defined by the oxidant/cooling subsystem design. These factors are the air mass required for oxidant reaction, the heat generated by the stack, the air flow needed for cooling the stack and the fan operating point.

Based on Table 7, we can see that air required by oxidant reaction increases when current rises, and it is much lower than the air flow required for cooling the stack. It is proved that in all the cases, the stoichiometric rate keeps inside the range recommended by the manufacturer (50–200). Additionally, we can observe that the less efficient configuration (#1) is the one that implies highest heat production in the stack. From this, configuration 2 and 3 reduces gradually the heat generation, and therefore the air required for cooling decreases too.

Regarding the fan speed, it is adjusted according to the control algorithm. The fan operating point can be known taking into account the pressure drop that the air flowing through the stack experiences and the air flow needed for cooling. Fig. 18a and b shows the fan/s operating range, in the three cases, is inside of nominal operating area defined by the fan manufacturer.

Where (equations expressed below have been obtained from manufacturer data [29,30],

- $Air_{stack} = 0.000996 \cdot I_s \cdot n_{cell}$ is the air flow required for oxidant reaction (m^3/h).
- $Q_{stack\_heat} = n_{cell} \cdot (1.25\ V - V_{cell}) \cdot I_s$ is the heat generated by the stack (W).
  - o n_{cell} is the number of cells that integrates the stack (80).
  - o $V_{cell} = V_{stack}/n_{cell}$ is the cell voltage (V).
  - o I_s is the number stack current (A).
- $\dot{V}_s = \frac{Q_{stack\_heat}}{(T_s - T_{amb}) \cdot C_p \cdot \rho_{air}}$ is the air volume flow needed for stack cooling (m^3/h).
  - o T_s is the stack temperature (ºC).
  - o T_{amb} is the ambient temperature (23 °C).
  - o C_p is air heat capacity (1012 J/(Kg·K)).
  - o ρ_{air} is the air density (1.29 kg/m^3).
- $\Delta P = \cdot P_s + \cdot P_{ducting}$ is the total pressure drop that the air flowing experiences (Pa).
  - o $P_s = \frac{0.0592 \cdot (T_s+273)^{1.5}}{T_s+393} \cdot \frac{\dot{V}_s}{(n_{cell}+1)}$ is the pressure drop through the stack (Pa), with $\dot{V}_s$ expressed in l/min.
  - o $P_{ducting}$ is the ancillary air pressure drop such as the ducting (no higher than 24 Pa)

Before to conclude, we are going to compare the performances obtained from each configuration with the standard configuration recommended by the manufacturer. Then, Fig. 19a shows the stack voltage obtained in each case, and from it, we can deduce the configuration that allows obtaining the best performance from the stack is the one that guarantees the best breathing/cooling to the stack (configuration 3). Fig. 19b shows that configuration 3 allows extracting from the stack more power than the power offered according to standard configuration proposed by manufacturer.

The last comparison is related to stack temperature. As we can observe from Fig. 19c, those configurations where the stack is properly cooled, the stack temperature is very close to optimal temperature and it matches with configurations that offer higher power rates. As a result, worse temperature control involves worse stack performance.[1]

Finally, Table 8 summarizes the main characteristics of the proposed configurations and the standard configuration proposed by the manufacturer, attending to parameters for accomplishing the challenges posed as goals of the presented work in relation to the oxidant/coolant subsystem. These parameters are:

- Number of fans which integrate the subsystem.
- Size of the enclosure.
- Total weight.
- Cost, calculated as unitary cost * number of units.
- Auxiliary power consumption, calculated as unitary power consumption * number of units.
- Possibility of airflow control.
- Homogenous temperature distribution. Taking into account the stack in made up by 80 cells, the maximum difference between the hottest and coldest point to consider the temperature distribution as uniform is fixed at 2 °C; this corresponds with a rate of 0,025 °C/cell
- And finally, fuel cell system efficiency, calculated as “Output Electrical Power/Hydrogen Consumed)

In basis of them, Table 8 offers a comparative of requirements achieved by each proposal, showing that configuration 3 accomplishes all of them.

[1] Regarding stack temperature response, differences at the beginning of each test are justified because stack has been subjected to different initial conditions.

Table 8
Summary of the performances obtained from the proposed Oxidant/Cooling subsystems and from the manufacturer standard configuration.

Configuration	Structure	Number of fans	Size (W x L x H) (mm)	Weight (gr)	Cost (€)	Auxiliary Power Consumption (W)	Air flow Control	Homogenous Temperature Distribution	AC-PEFC Efficiency (Electrical power/H2 consumption)
1	Four fans without control 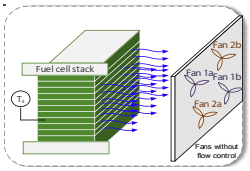 meter, adjusted slightly below	4	400 × 200 × 600	3280	799.36	364.8	No	No	30%
2	Four fans with control 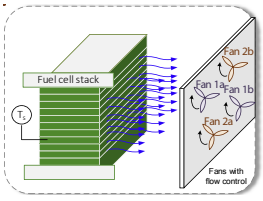	4	400 × 200 × 600	3280	799.36	364.8	Yes	No	42%
3	One single speed controlled fan 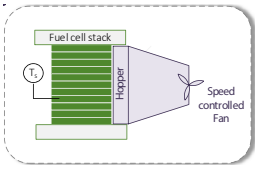	1	350 × 250 × 440	820	199.84	91	Yes	Yes	50%
Manufacturer proposal	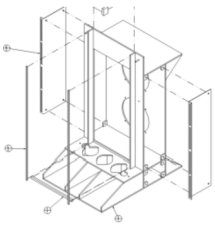	2	400 × 200 × 600	410	399.7	182.4	No	No	45%

6. Conclusion

This paper presents a comprehensive experimental study of three possible configurations of the Oxidant/Cooling subsystem in an AC-PEFC. This presented study justifies that the authors are trying to enhance the Oxidant/Cooling subsystem. Contrary to what one might think, and based on experimental results, this paper has shown how the Oxidant/Cooling subsystem can condition the stack operation. It is really important to control the stoichiometric rate between the values recommended by the manufacturer's data to avoid the stack deterioration.

This work departs from six challenges in the design and manufacture of the oxidant/cooling sub-system in an AC-PEFC: 1) to be able to cool the stack homogeneously, 2) to provide sufficient airflow range to control the PEFC temperature, under a range of power and room/coolant air temperature, 3) to place the stack at optimum temperature, 4) to reduce the auxiliary power consumption, 5) to do all this within a certain sized box, and last but not least 6) to do so cost effectively.

In order to overcome the challenges posed, the presented work departs from a configuration based on manufacturer recommendations and trying to improve the stack temperature control including some changes which could make to enhance the system operation.

To carry out the study, different configurations for the Oxidant/Cooling subsystem have been designed, built and analysed based on the AC-PEFC responses. Proposed configurations are based on influencing on different devices which integrate the Oxidant/Cooling subsystem (fan/s, distance, enclosure design, flow adapter, and so on). Different variables have been analysed from the AC-PEFC system with the different configurations applied to the Oxidant/Cooling subsystem. This has been complemented by introducing different thermography at different stack current values to study the temperature distribution over the stack cathode area.

Three configurations have been carried out: four fans covering the cathode area of the stack working two by two without flow control, four fans covering the cathode area of the stack working two by two with flow control, and one single fan with speed controlled. The first two are housed in a polycarbonate rectangular-shaped enclosure that covers the entire stack. The third has been placed in a cone-shaped hopper also covering the entire stack. This cover is adapted to the stack geometry.

With regard to the experimental results, we can assert that the first two proposals present a diminished airflow distribution because the airflow follows preferential paths due to the space. This space is found between the polycarbonate enclosure and the stack, and the airflow follows these paths instead of crossing the stack and cooling it.

References

[1] F. Barbir, PEM Fuel Cells: Theory and Practice, Elsevier Academic Press, New York, 2012.
[2] U. Kunze, J. Paschos, O. Stimming, Fuel Cell Comparison to Alternate Technologies, in Fuel Cells, Springer, 2013, pp. 77–95.
[3] EG&G Technical Services, Fuel cell handbook, seventh, U.S: Department of Energy, 2004, p. 427.
[4] M. Andersson, S.B. Beale, M. Espinoza, Z. Wu, W. Lehnert, A review of cell-scale multiphase flow modeling, including water management, in polymer electrolyte fuel cells, Appl. Energy 180 (2016) 757–778.
[5] D. Guida, M. Minutillo, Design methodology for a PEM fuel cell power system in a more electrical aircraft, Appl. Energy (Nov. 2016).
[6] M.J. Vasallo, J.M. Bravo, J.M. Andújar, Optimal sizing for UPS systems based on batteries and/or fuel cell, Appl. Energy 105 (2013) 170–181.
[7] F. Segura, E. Durán, J.M. Andújar, Design, building and testing of a stand alone fuel cell hybrid system, J. Power Sources 193 (2009) 276–284.
[8] S. Cordiner, V. Mulone, A. Giordani, M. Savino, G. Tomarchio, T. Malkow, G. Tsotridis, A. Pilenga, M.L. Karlsen, J. Jensen, Fuel cell based Hybrid Renewable Energy Systems for off-grid telecom stations: data analysis from on field demonstration tests, Appl. Energy (2016).
[9] J.J.B.M.J. Vasallo, J.M. Andújar, C. García, A methodology for sizing backup fuel-cell/battery hybrid power systems, Ind. Electron. IEEE Trans. 57 (6) (2010) 1964–1975.
[10] F. Segura, J.M. Andújar, Power management based on sliding control applied to fuel cell systems: a further step towards the hybrid control concept, Appl. Energy 99 (2012) 213–225.
[11] A. Gomez, A. Raj, A.P. Sasmito, T. Shamim, Effect of operating parameters on the transient performance of a polymer electrolyte membrane fuel cell stack with a dead-end anode, Appl. Energy 130 (2014) 692–701.
[12] G. Zhang, S.G. Kandlikar, A critical review of cooling techniques in proton exchange membrane fuel cell stacks, Int. J. Hydrogen Energy 37 (3) (2012) 2412–2429.
[13] J.W. Ahn, S.Y. Choe, Coolant controls of a PEM fuel cell system, J. Power Sources 179 (2008) 252–264.
[14] H.S. Han, C. Cho, S.Y. Kim, J.M. Hyun, Performance evaluation of a polymer electrolyte membrane fuel cell system for powering portable freezer, Appl. Energy 105 (2013) 125–137.
[15] A.P. Sasmito, E. Birgersson, K.W. Lum, A.S. Mujumdar, Fan selection and stack design for open-cathode polymer electrolyte fuel cell stacks, Renew. Energy 37 (1) (2012) 325–332.
[16] F. Segura, J.M. Andújar, Step by step development of a real fuel cell system. Design, implementation, control and monitoring, Int. J. Hydrogen Energy 40 (15) (2015) 5496–5508.
[17] F. Philipps, G. Simons, K. Schiefer, Dynamic investigation of PEFC stacks in interaction with the air supply system, J. Power Sources 154 (2) (Mar. 2006) 412–419.
[18] Y.-B. Kim, Improving dynamic performance of proton-exchange membrane fuel cell system using time delay control, J. Power Sources 195 (19) (2010) 6329–6341.
[19] O. Himanen, T. Hottinen, S. Tuurala, Operation of a planar free-breathing PEMFC in a dead-end mode, Electrochem. Commun. 9 (2007) 891–894.
[20] R. Eckl, W. Zehtner, C. Leu, and U. Wagner, “Experimental analysis of water management in a self-humidifying polymer electrolyte fuel cell stack,” J. Power Sources, vol. 138, no. 1–2, pp. 137–144.
[21] H.-W. Wu, A review of recent development: transport and performance modeling of PEM fuel cells, Appl. Energy 165 (2016) 81–106.
[22] R.C. Samsun, J. Pasel, H. Janßen, W. Lehnert, R. Peters, D. Stolten, Design and test of a 5 kWe high-temperature polymer electrolyte fuel cell system operated with diesel and kerosene, Appl. Energy 114 (2014) 238–249.
[23] M. Gerbec, V. Jovan, J. Petrovčič, Operational and safety analyses of a commercial PEMFC system, Int. J. Hydrogen Energy 33 (2008) 4147–4160.
[24] U. Soupremanien, S. Le Person, M. Favre-Marinet, Y. Bultel, Tools for designing the cooling system of a proton exchange membrane fuel cell, Appl. Therm. Eng. 40 (2012) 161–173.
[25] J. Marcinkoski, B.D. James, J. a Kalinoski, W. Podolski, T. Benjamin, J. Kopasz, Manufacturing process assumptions used in fuel cell system cost analyses, J. Power Sources 196 (12) (2011) 5282–5292.
[26] B.J. Kim, M.S. Kim, Studies on the cathode humidification by exhaust gas recirculation for PEM fuel cell, Int. J. Hydrogen Energy 37 (5) (2012) 4290–4299.
[27] Q. Meyer, A. Himeur, S. Ashton, O. Curnick, R. Clague, T. Reisch, P. Adcock, P.R. Shearing, D.J.L. Brett, System-level electro-thermal optimisation of air-cooled open-cathode polymer electrolyte fuel cells: air blower parasitic load and schemes for dynamic operation, Int. J. Hydrogen Energy 40 (no. 46) (2015) 16760–16766.
[28] Q. Wu, H. Li, W. Yuan, Z. Luo, F. Wang, H. Sun, X. Zhao, H. Fu, Performance evaluation of an air-breathing high-temperature proton exchange membrane fuel cell, Appl. Energy 160 (2015) 146–152.
[29] FCgen ® -1020ACS/FCvelocity ® -1020ACS Fuel Cell Stack. Product Manual and Integration Guide, 2010.
[30] Ballard Putting Fuel Cells to Work FCgen ® -1020ACS Fuel Cell Stack FCvelocity ® -1020ACS Fuel Cell Stack Product Manual and Integration Guide, 2014.
[31] Ebmpapst, Product Data Sheet DV6224 TDA, 2012.